



Article

Provenance analysis of sediments in the south-east Aegean during the Upper Quaternary: a composite approach based on bulk and clay mineralogy and geochemistry

Georgia Leontopoulou¹, Georgios E. Christidis^{1*} , Grigorios Rousakis², Noémi S. Müller³, George Papatheodorou⁴ and Maria Geraga⁴

¹Technical University of Crete, School of Mineral Resources Engineering, 73100 Chania, Greece; ²Hellenic Center for Marine Research, Institute of Oceanography, 46,7Km Athens-Sounio Av. Mavro Lithari, PO Box 712, 19013, Anavissos, Attica, Greece; ³Fitch Laboratory, British Archaeological School at Athens, Souedias Street 52, 10676 Athens, Greece and ⁴University of Patras, Department of Geology, 26500 Rio, Patras, Greece

Abstract

Sediments from the ST5 deep-sea bottom core collected from the south-east Aegean Sea between Symi and Tilos islands, Greece, were examined by quantitative mineralogical analysis and geochemical analysis to infer provenance and palaeoenvironmental control over sediment deposition. The mineralogical composition comprises carbonates (mainly calcite and Mg-calcite), quartz, feldspars, serpentine, amphibole and clay minerals. Chlorite is the most abundant clay mineral, whereas smectite and illite are less abundant than in the sediments in the south-west Aegean and the Cretan Sea. Semi-quantitative analysis of clay minerals from oriented clay fractions overestimates significantly the smectite content and underestimates the abundances of illite, chlorite and kaolinite. The studied sediments are enriched in MgO, Ni and Cr, which decrease in abundance with decreasing depth, following the distribution of serpentine. By contrast, the abundances of SiO₂, Al₂O₃, Fe₂O₃, Na₂O and K₂O increase upcore. The regional S1 sapropel horizon is enriched in V and Co and has considerably greater Ba/Al ratios than the remaining sequence. The mineralogical and geochemical relationships indicate a strong ultrabasic influence, probably from the Marmaris ophiolite in the Lycian nappes. The clay mineral distribution suggests that the smectite was mainly of volcanogenic origin, the illite was supplied by the nearby landmasses of west Anatolia and the islands of Rhodes, Tilos and Symi and the contribution from the south-east Mediterranean was limited or totally lacking. The combined use of the mineralogical and geochemical analysis of bulk sediments rather than the clay fractions is not only extremely useful in tracing sediment provenance in relatively closed basins, but it also enables a more realistic assessment of the importance of water circulation patterns on sedimentation processes in such environments.

Keywords: Aegean Sea, clay minerals, mineralogical composition, provenance, Rietveld analysis, ultrabasic rocks

(Received 9 August 2021; revised 27 December 2021; Accepted Manuscript online: 7 January 2022; Associate Editor: Warren D. Huff)

The provenance of the fine-grained suspended particulate matter (SPM) of marine hemipelagic sediments is of particular importance in sedimentological studies because it provides information about the sedimentary processes that control transport and deposition. Sedimentary variability heavily depends on provenance, but it is also affected by climatic factors (e.g. climate change) and in the Anthropocene (cf. Zalasiewicz *et al.*, 2011) by human activities. This provenance may be determined from mineralogical analysis of the clay minerals that are associated with variable weathering processes, which in turn are linked with climatic variations through geological time (e.g. Vanderaveret *et al.*, 1999; Thiry, 2000; Bout-Roumazielles *et al.*, 2007; Adriaens *et al.*, 2018, among many others). Therefore, clay minerals in recent

marine and terrestrial sedimentary successions have received considerable interest in palaeoclimatic and palaeoceanographic studies (Martinez-Ruiz *et al.*, 2000; Dera *et al.*, 2009; Sabatier *et al.*, 2010; Ergin *et al.*, 2012; Garzanti *et al.*, 2014; Lister *et al.*, 2015). This is because in such environments and ages of sediment the distribution of clay minerals is not affected significantly by diagenesis but is determined by the existence of multiple sources, the differential stability of clay minerals to alteration, potential climatic variations, the maturity of soil profiles and transport routes and depositional processes (Thiry, 2000).

Provenance and palaeoclimatic interpretations using clay minerals are based on using semi-quantitative methods. The semi-quantitative approaches have several shortcomings (e.g. Leontopoulou *et al.*, 2019), and recently, more complex methods have been employed that utilize X-ray diffraction (XRD) profile modelling of the clay fractions with specialized computer codes (Zeelmaekers *et al.*, 2015; Kemp *et al.*, 2016; Adriaens *et al.*, 2018). In an attempt to overcome the shortcomings of the semi-quantitative methods, which, among other shortcomings,

*E-mail: christid@mred.tuc.gr

Cite this article: Leontopoulou G, Christidis GE, Rousakis G, Müller NS, Papatheodorou G, Geraga M (2021). Provenance analysis of sediments in the south-east Aegean during the Upper Quaternary: a composite approach based on bulk and clay mineralogy and geochemistry. *Clay Minerals* 56, 229–249. <https://doi.org/10.1180/clm.2022.2>

overestimate significantly the smectite contents of sediments, Leontopoulou *et al.* (2019) proposed a novel approach. This approach is based on the analysis of the bulk sediments coupled with the bulk geochemistry of the sediments and specialized tests on the oriented clay fractions (heating at 530°C followed by ethylene glycol (EG) solvation), rather than the semi-quantitative estimation of clay minerals from oriented clay fractions. The combination of quantitative bulk mineralogical analysis with bulk geochemistry was used in the past in sediments offshore from Brazil (Kronberg *et al.*, 1986). However, the mineralogical analysis was normative as it was calculated from the chemical composition of the sediments (cf. Kronberg *et al.*, 1986). Moreover, the thermal characteristics of individual clay minerals and their possible significance for data interpretation were not considered.

The clay mineralogical composition of Aegean marine sediments has been studied extensively in the past, being heavily reliant on semi-quantitative analysis (Aksu *et al.*, 1995a; Bayhan *et al.*, 2001; Karageorgis *et al.*, 2005; Ehrmann *et al.*, 2007, 2013; Ergin *et al.*, 2007, 2012; Poulos, 2009). These studies consider the Nile-derived sediments as an important component of the sediments in the south-east Aegean (cf. Ehrmann *et al.*, 2007, 2013; Poulos 2009). However, in a recent study we showed that the contribution of south-east Mediterranean SPM to the sediments of the eastern Cretan Sea and the south-west Aegean Sea is negligible (Leontopoulou *et al.*, 2019). In the present contribution we examine the provenance of sediments of the ST5 core in the south-east Aegean Sea (Fig. 1) following the same analytical approach and protocols for the bulk sediments and the clay fractions. This particular core was selected because of its excellent location in the area where the south-east Mediterranean Sea meets the Aegean region. Therefore, any contribution from the south-east Mediterranean, as has been postulated in previous studies (Ehrmann *et al.*, 2007, 2013; Poulos, 2009), if it exists, might be traced and verified, thus testing the sensitivity of the approach.

The south Aegean Sea links the Levantine Basin and the Ionian Sea through the eastern and western straits of the Cretan Arc (Fig. 1) (Lykousis *et al.*, 2002). The upper sea layer is probably occupied by the Modified Atlantic Water originating from the Ionian Sea, the Levantine Surface Waters (LSWs) originating from the Levantine Sea and the Black Sea Water from the north. Three water masses occupy the intermediate and deep waters of the area: the Cretan Intermediate Water formed locally; the Transitional Mediterranean Water coming through the eastern and western Cretan Arc Straits; and the Cretan Deep Water formed locally. In addition, the dense north Aegean water sinks, flows to the south Aegean Sea and then is directed to the eastern Mediterranean Sea through the Cretan Straits, contributing to the rejuvenation of the bottom water (Tripsanas *et al.*, 2016). Within this context, the south-east Aegean Sea displays two main differences compared to the Cretan Sea and the south-west Aegean Sea: firstly, it is bordered by the estuaries of several rivers, which drain the nearby west Anatolian landmass; and secondly, circulation patterns in the south-east Aegean Sea are different from those of the Cretan Sea and the south-west Aegean Sea. The south-east Aegean Sea is dominated by the LSWs originating from the south-east Mediterranean Sea, which thus might contribute to the composition of sediments in the area, as has been proposed in the past (Ehrmann *et al.*, 2007, 2013; Poulos, 2009). On the other hand, the Cretan Sea is dominated by rotating currents (Cretan Sea gyres) within the basin with limited input from the south-west and south-east Aegean Sea (Lykousis *et al.*, 2002). Finally, the south-west Aegean Sea is characterized by the dense north

Aegean water that transports SPM from the north and central Aegean Sea and the presence of the Myrtoan Sea Gyre (Lykousis *et al.*, 2002; Tripsanas *et al.*, 2016).

This paper re-examines the clay mineral relationships proposed in previous studies in the south-east Aegean area, discusses sediment provenance and interprets the bulk and clay mineralogy and geochemistry according to the existing palaeoclimatic and palaeoceanographic models for the broader area, considering the various sedimentological settings in the various Aegean areas. In addition, the role of Asia Minor vs the Nilotic region as regards the provenance of SPM in the south-east Aegean Sea is discussed.

Materials and methods

Core sampling and sample preparation

The present study focuses on the analysis of sediment samples obtained from the ST5 gravity core (36°30.752'N, 27°41.511'E, water depth 688 m, length 381 cm) recovered during a Research Vehicle of the Hellenic Center for Marine Research oceanographic cruise on 20 June 2011 near Symi Island, south-east Aegean Sea (Fig. 1). The gravity core was split longitudinally and we received one half of the core, which was photographed and described macroscopically at the laboratory. A total of 59 subsamples were collected for mineralogical and geochemical analysis from the half-core, each consisting of ~4 g of dried material. Before the analyses, the samples were washed repeatedly with deionized water to remove soluble salts until electric conductivity was <50 $\mu\text{S m}^{-1}$. The gravity core contains a dark-coloured mud unit that corresponds to sapropel S1, which was subsequently confirmed by organic carbon (C_{org}) analysis. Sapropel S1 consists of two discrete intervals, referred to hereafter as the lower (S1a) and upper (S1b) layers, which are separated by an interval of lighter colour corresponding to the S1 interruption caused by re-ventilation of large parts of the basin (Geraga *et al.*, 2000; Mercone *et al.*, 2001; Gogou *et al.*, 2007; Triantaphyllou *et al.*, 2009).

Grain-size analysis

Grain-size analysis was carried out on the bulk samples using laser diffraction on dilute suspensions of the washed samples with a Mastersizer S (Malvern Instruments), without the use of a deflocculant. The proportions (%) of sand, silt and clay fractions were calculated according to the Udden–Wentworth scale (Wentworth, 1922) from the cumulative size distributions provided from the particle-size analyses. The classification of sediments was conducted according to the approach of Folk (1974).

Mineralogical analysis

The mineralogical composition of the sediments was examined using XRD with a Bruker D8 Advance diffractometer equipped with a Lynx-eye silicon strip detector, using Ni-filtered Cu-K α radiation (40 kV, 40 mA), 0.298° divergence and anti-scatter slits, as well as a step size of 0.019°2 θ , with a 63.5 s count time per step. Data were evaluated using the EVA® software provided by Bruker. The bulk mineralogy was determined on random powders prepared after grinding of the sediments by hand with an agate pestle and mortar in acetone medium, subsequent drying at 60°C and mounting by careful side loading onto Al holders

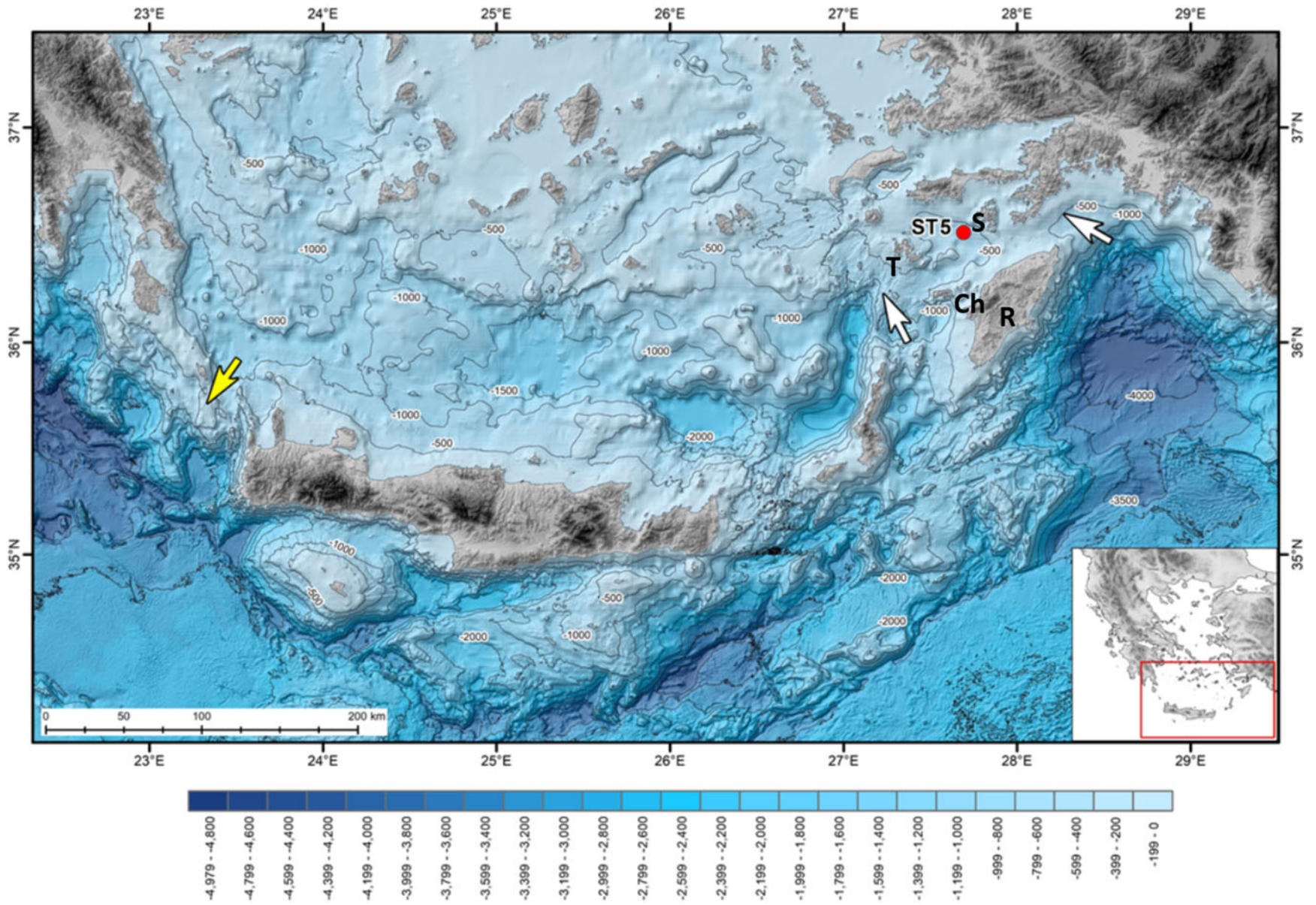


Fig. 1. Location of the investigated core ST5. The arrows indicate the eastern (white arrows) and western (yellow arrow) straits of the Cretan Arc. Ch = Chalki Island; R = Rhodes Island; S = Symi Island; T = Tilos Island.

to avoid preferred orientation. The final particle size of the sediments analysed by XRD was $\sim 3 \mu\text{m}$ (tested by laser diffraction). The clay mineralogy was determined from $< 2 \mu\text{m}$ fractions of the as-received samples separated from suspension by differential settling according to Stoke's Law and then spread onto glass slides to form oriented mounts and allowed to dry in air. The carbonates were not dissolved from the clay fraction in an attempt to verify the possible differentiation of the various carbonate phases in that fraction (see 'Results' section). The clay minerals were identified from air-dried (AD) and EG-solvated slides, as well as slides heated at 530°C . In addition, ~ 40 separate aliquots of the heated slides were subsequently EG-solvated. This allowed for differentiation of the dioctahedral smectites with low dehydroxylation temperatures (Fe-montmorillonite, nontronite and/or beidellite) from dioctahedral smectites with higher dehydroxylation temperatures (Drits *et al.*, 1998). The EG-solvated slides were used to determine the abundances of smectite, illite, kaolinite and chlorite according to the approach of Biscaye (1965). In brief, the approach uses the integrated areas of the 001 basal reflections of smectite, illite and kaolinite and the area of the 002 basal reflection of chlorite, which are multiplied by suitable factors and normalized to 100%. Finally, the 7 \AA peak is divided between kaolinite and chlorite in proportion to the fractions of these minerals, calculated from the areas of the 002 peak of kaolinite and of the 004 peak of chlorite at $\sim 25^\circ 2\theta$.

The mineral phases in the bulk sediments were quantified using a Rietveld-based refinement routine with the BGMN code (*Autoquan*[®] software version 2.80; Seifert). The Rietveld method compares the full experimental profile with the calculated XRD profile, with each data point (2θ step) being an independent observation. Although it was originally used for the structure refinement of minerals (cf. Post & Bish, 1989), it has evolved to become an efficient and reliable method for the quantitative analysis of soft sediments and industrial minerals (Snellings *et al.*, 2010; Bish & Plötze, 2011; Karageorgis *et al.*, 2012; Adriaens *et al.*, 2018; Leontopoulou *et al.*, 2019). Due to the small amount of material in each sample extracted originally from the half-core and the need to perform several analyses from this small sample, the addition of an internal standard was not performed to estimate the error of the method. However, Leontopoulou *et al.* (2019) recently used a ZnO internal standard to estimate the absolute error (estimation of accuracy) of the quantitative determinations in similar Aegean sediments. The error estimated from the internal standard was $\pm 0.5\%$ at 15% abundance ($\sim 3.4\%$ relative error). The reproducibility (estimation of precision) of the quantitative analyses, estimated from duplicate analyses of representative samples, was better than $\pm 2\%$ for abundances of $> 10\%$, $\pm \sim 4\%$ for abundances of 5–10%, $\pm \sim 7\%$ for abundances of 1.5–5.0% and $\pm \sim 10\%$ for abundances of $< 1.5\%$. A detailed description of the analytical approach was given by Leontopoulou *et al.* (2019). An independent estimation of the accuracy of the determination of total carbonate contents (calcite, Mg-calcite, aragonite and dolomite) was obtained from X-ray fluorescence (XRF) analysis of the bulk sediments (see 'Results' section).

Finally, the abundances of smectite, illite, kaolinite and chlorite determined using the Rietveld approach were normalized to 100% and were compared with those obtained from the semi-quantitative approach of Biscaye (1965) described previously.

Geochemical analysis

All sediment samples were analysed for major and trace elements using wavelength-dispersive XRF spectroscopy with a S8 Tiger

XRF spectrometer with a Rh excitation source (Bruker), using a custom calibration based on 43 certified reference materials, which had been developed for the analysis of soils and ceramics prepared as glass beads (Georgakopoulou *et al.*, 2017). Loss on ignition (LOI) was determined by placing $\sim 2 \text{ g}$ of pulverized, dried sample in a porcelain crucible and heating to 1050°C for 2 h in a muffle furnace. Glass beads were subsequently prepared on an automatic fluxer with 1.5 g of the ignited sample and 7.5 g of a mixture of lithium metaborate/lithium tetraborate.

Organic carbon (C_{org} ; wt.%) was determined for all samples by means of a CHNS-O elemental analyser (LECO). Carbonates were removed previously by dissolution with 1 N HCl, stirring for 2 h and subsequent washing of the sediments with distilled water and drying at 60°C . Aliquots of 10–15 mg of the samples were introduced into the CHNS-O analyser.

Radiocarbon dating and age model

The chronostratigraphy of the core is based on four accelerator mass spectrometry (AMS) ^{14}C ages. The analyses were performed by Beta Analytic Laboratories in Florida (USA) on cleaned, hand-picked planktonic foraminifera. Conventional ^{14}C ages were calibrated with the CALIB v. 5.0.2 program (Stuiver & Reimer, 1993; Stuiver *et al.*, 1998) and the MARINE04 ^{14}C calibration dataset for 1σ intervals (Hughen *et al.*, 2004). Regional reservoir age corrections (ΔR) of 149 ± 30 years for sapropel intervals (Facorellis *et al.*, 1998) and of 58 ± 85 years outside the sapropel (Reimer & McCormac, 2002) were applied.

Scanning electron microscopy

The clay fractions of selected samples were gold-coated and were studied using scanning electron microscopy (SEM) with a JEOL 6400 microscope equipped with an energy-dispersive spectrometer (EDS) and a wavelength-dispersive spectrometer.

Core description

Five lithological units were identified in core ST5 based on the colour, grain size, C_{org} and sedimentary structures (Fig. 2). The first unit (0–5 cm) consists of dull yellow, oxidized, water-rich mud. The second unit (5–58 cm) consists of greyish-olive water-rich mud. The third unit (58–141 cm) consists of olive-grey plastic mud with sporadic organic matter-rich lenses. The fourth unit (141–185 cm) corresponds to the sapropel sequence (sapropel S1) and consists of darker olive-grey sapropelic mud. The sapropel S1 deposition has been divided in two dark sublayers: S1a and S1b (S1a: 165–185 cm; S1b: 141–160 cm below sea floor (bsf)). Between these two sapropel sublayers is the characteristic distinct interruption of sapropel S1 at 160–165 cm. Within the sapropel sequence, the maximum C_{org} content (1.77%) occurs at 175.5 cm. The fifth unit (185–381 cm) is a stiff olive-grey mud differentiated from the previous unit by a colour transition from olive-grey 2,5GY 5/1 to olive-grey 5GY 5/1.

Results

Grain size

The downcore grain-size distribution of core ST5 is shown in Fig. 2. The sediments consist of clay (28–89%, average 60%) and silt (11–62%, average 39%), while the sand content does

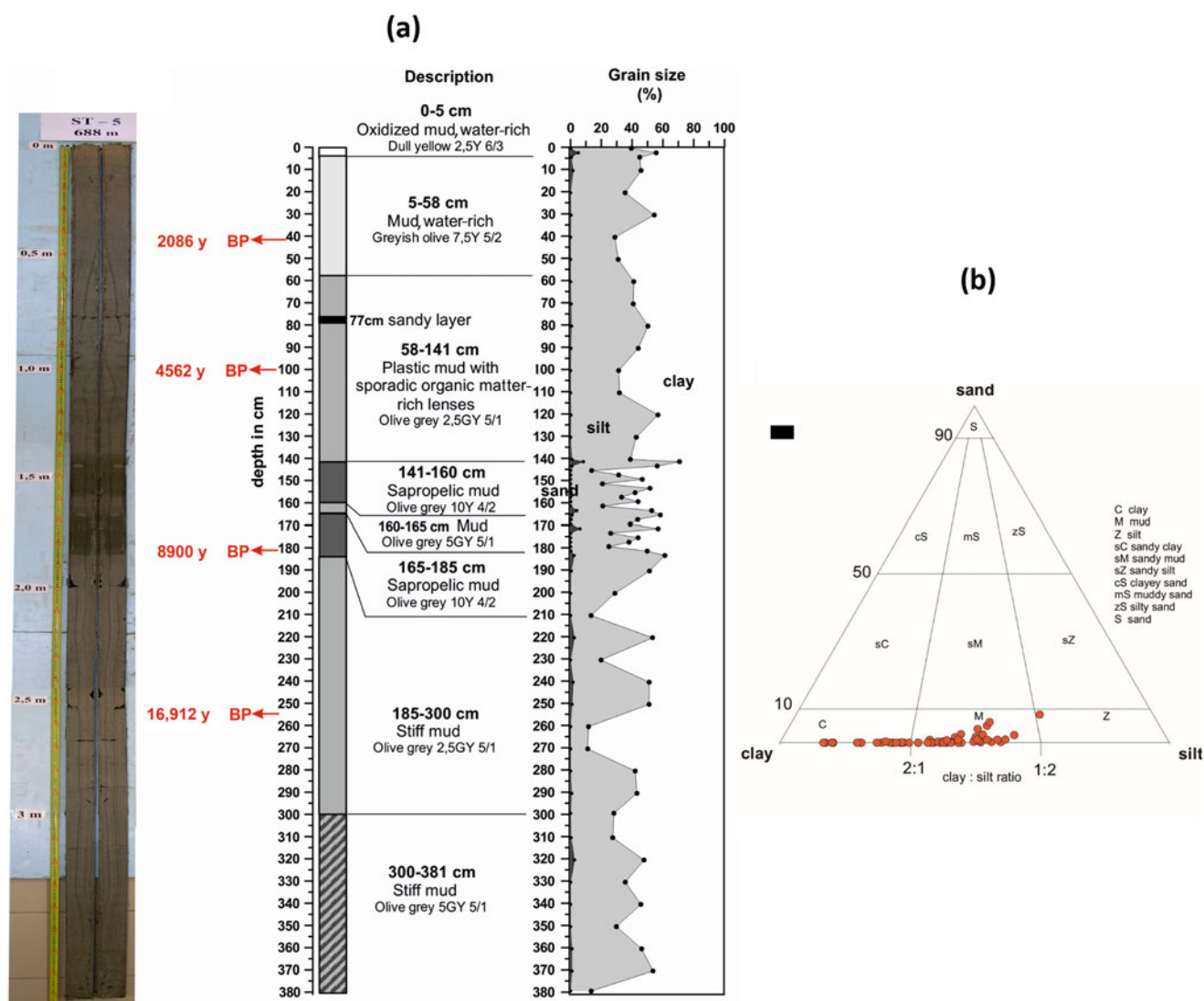


Fig. 2. (a) Description of lithological units and downcore evolution of the sediment size fractions of core ST5. The darker areas indicate sapropel S1. The vertical axis denotes the depth bsf. (b) Classification of the ST5 sediments according to the Folk (1974) scheme.

not exceed 10% (average 1%). The studied sediments are fine-grained, with the silt + clay fractions exceeding 94%, while the average median particle size (D_{50}) is 5.1 μm . The clay content increases with depth, while the sand content does not show significant differentiation. No particular trend was observed in the distribution of the silt fraction. According to Folk's (1974) classification scheme, the sediments are classified as muds and clays (Fig. 2b). The D_{50} values in this core also remain within the range of fine-grained silt (<7.8 μm) according to the Udden-Wentworth scale, and the distribution of D_{50} tends to decrease with depth, similar to the clay content. In addition, D_{50} tends to decrease in the top of the sapropelic layer S1b, while the sand content increases in the S1 horizon. Thus, most of the sapropel samples are coarser in general compared to the surrounding sediments (Fig. 2). By contrast, the pre- and post-sapropel sediments cannot be clearly differentiated based on their grain size.

Bulk mineralogy

The downcore distribution of major minerals is depicted in Fig. 3 and a summary of the results (average concentrations, standard

deviations, minimum and maximum values) is listed in Table 1. Representative XRD traces are shown in Fig. S1, and the mineralogical compositions of all samples are listed in Table S1. The bulk mineralogical compositions comprise mainly carbonate minerals (calcite, Mg-calcite, aragonite and dolomite), ranging from 32.5 to 43.9% in total. Calcite ranges between 17.2 and 26.6 wt.% (average 22.1 wt.%), Mg-calcite ranges between 5.2 and 12.0 wt.% (average 8.1 wt.%), quartz ranges between 10.2 and 15.7 wt.% (average 12.6 wt.%) and feldspars range between 5.3 and 13.3 wt.% (average 8.8 wt.%). Chlorite is the most abundant clay mineral and ranges between 7.0 and 14.5 wt.% (average 10.1 wt.%), illite ranges between 3.2 and 11.4 wt.% (average 7.8 wt.%), kaolinite ranges between 3.2 and 7.2 wt.% (average 5.1 wt.%), smectite ranges between 0.5 and 7.1 wt.% (average 3.0 wt.%) and palygorskite ranges between 1.4 and 3.3 wt.% (average 2.0 wt.%). The biogenic component of the sediments is composed mainly of calcite, Mg-calcite and aragonite. In the sediments, hornblende ranges between 2.5 and 5.5 wt.% (average 3.7 wt.%), and it occurs together with serpentine and talc as accessory mineral phases, indicating input from an ultrabasic component, while pyrite is a trace phase. The main phases in the sediment samples comprise

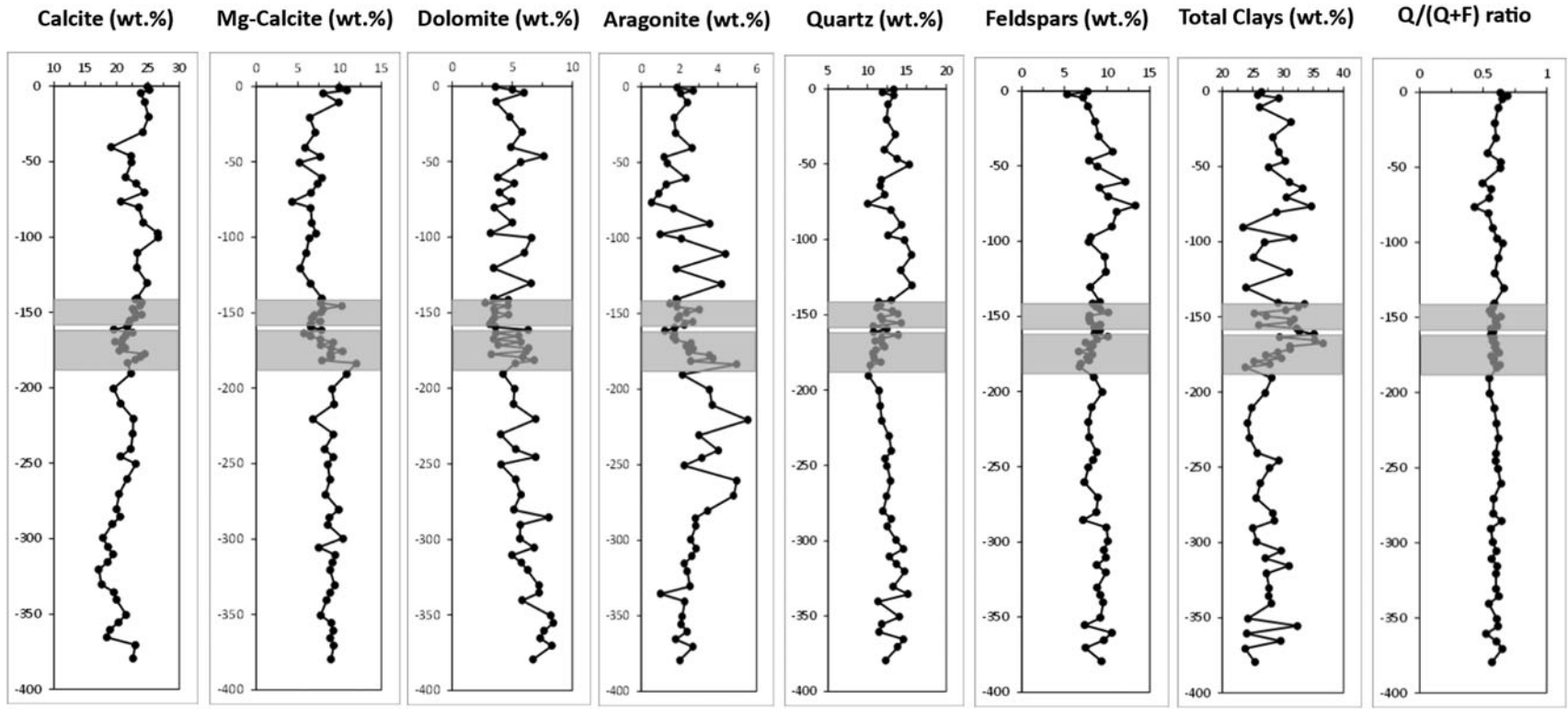


Fig. 3. Downcore variation of major minerals (wt.%) in core ST5 determined using the Rietveld method. The shaded areas indicate sapropel S1. The vertical axes denote the depth bsf.

Table 1. Mineralogical composition of core ST5.

Minerals	Holocene sediments above sapropel S1				Sapropel S1				Holocene sediments below sapropel S1			
	Mean (wt.%)	SD	Min. (wt.%)	Max. (wt.%)	Mean (wt.%)	SD	Min. (wt.%)	Max. (wt.%)	Mean (wt.%)	SD	Min. (wt.%)	Max. (wt.%)
Calcite	23.8	1.7	19.1	26.6	22.2	1.4	19.6	24.5	20.6	1.9	17.2	23.1
Mg-calcite	7.2	1.7	5.2	10.9	8.1	1.5	5.7	12.0	9.0	0.9	6.8	10.8
Dolomite	4.8	1.1	3.5	6.6	4.5	1.3	2.8	6.8	5.9	1.3	4.0	8.3
Aragonite	2.3	1.0	0.9	4.4	2.4	0.9	1.2	5.0	3.1	1.0	2.0	5.6
Palygorskite	2.0	0.5	1.4	3.3	2.3	0.4	1.6	3.1	1.8	0.2	1.4	2.3
Smectite	3.7	0.9	1.8	4.9	3.9	1.4	1.6	7.1	1.5	0.7	0.5	3.5
Kaolinite	5.0	0.8	3.2	6.3	5.1	0.8	4.0	7.2	5.1	0.4	3.9	5.7
Chlorite	9.9	2.3	7.0	14.5	9.8	1.9	7.1	12.4	10.5	1.6	7.2	13.0
Illite	7.4	1.7	3.2	9.8	9.1	1.4	6.3	11.4	7.0	0.8	5.7	8.9
Hornblende	3.5	0.4	2.9	4.1	4.2	0.7	3.2	5.5	3.3	0.4	2.5	4.4
Quartz	13.5	1.3	11.8	15.7	11.8	1.1	10.4	14.3	12.5	1.1	10.2	14.7
Plagioclase	5.7	1.2	2.8	7.3	5.0	0.6	4.0	6.0	5.8	0.8	4.1	7.0
Orthoclase	3.4	0.7	2.3	5.2	3.3	0.9	2.5	4.1	3.1	0.6	1.8	4.0
Paragonite	4.7	0.7	3.3	6.3	5.5	1.0	4.2	8.0	5.3	0.7	4.2	7.3
Lizardite	2.9	1.4	0.7	5.3	2.5	1.4	0.6	4.5	4.5	1.3	2.2	6.5
Q/Q+F	0.60	0.05	0.49	0.69	0.59	0.02	0.55	0.64	0.59	0.03	0.52	0.65

quartz and feldspars, accessory minerals from the ultrabasic component and clay minerals. Compared with the sediments that were studied by Leontopoulou *et al.* (2019), core ST5 displays three main differences (cf. Table 1 of this study with table 2 in Leontopoulou *et al.*, 2019): (1) it has considerably lower Mg-calcite and total carbonate contents but considerably greater dolomite contents; (2) it contains more chlorite, hornblende and serpentine, which underlines the contribution of an ultrabasic component, probably from the west Anatolian mainland; and (3) it has greater total clay mineral contents and quartz/(quartz + feldspar) (Q/Q+F) ratios.

The abundances of the various minerals display varying trends with increasing depth (Fig. 3). The abundances of dolomite and Mg-calcite tend to increase downcore, while that of calcite follows the opposite trend and that of aragonite remains constant in general throughout the core. The abundance of quartz tends to increase until the top of S1, then it decreases until the bottom of S1, where it reaches a minimum, and then it increases again at greater depths towards the bottom of the core. On average, the abundance of feldspars is generally constant throughout the core, whereas that of total clay minerals is constant on average in pre-sapropel S1 sediments, increases within sapropel S1 and remains generally constant in the post-sapropel S1 sediments (Fig. 3).

Serpentine displays a statistically significant overall positive correlation with chlorite ($r = 0.72$; Fig. 4a). This suggests the possibility for a common source and/or similar sedimentation processes for the two minerals. Two main subparallel trends are observed (Fig. 4): one for the pre-sapropel samples and a second one for the sapropel and post-sapropel sediments. In addition, the sediments from the upper sapropel horizon are generally richer in serpentine compared with their lower sapropelic counterparts. Moreover, a statistically significant overall negative correlation is observed between serpentine and illite ($r = -0.72$; Fig. 4b) and between chlorite and dolomite ($r = -0.84$ and -0.73 ; Fig. 4c). In the latter diagram two subparallel negative trends are observed, with the pre-sapropel S1 sediments having greater dolomite contents (Fig. 4c). Finally, clay minerals are inversely correlated with carbonates (Fig. 5a). The sapropelic sediments in general are richer in clay minerals than carbonates compared to the non-organic sediments. By contrast, the sapropelic sediments contain generally less quartz than their non-organic counterparts.

Furthermore, except for the S1 horizon, no particular trend is observed between clay minerals and quartz (Fig. 5b).

Clay mineralogy

The downcore distribution of clay minerals is depicted in Fig. 6, while the whole quantitative clay mineralogical dataset is listed in Table S2. An important characteristic of core ST5 compared to most Aegean areas is the presence of chlorite as the most abundant phyllosilicate (average 10.1 wt.%). The abundance of chlorite does not display a clear trend with depth. It is worth noting that illite and chlorite have a strong negative relationship, so in samples with large contents of illite there are small amounts of chlorite and *vice versa*. This is observed in almost the entire distribution of the core, except for the sapropel sequence, where this is less pronounced. Another noticeable feature of core ST5 is the lack of significant variations in the clay mineralogy of the sapropel horizon compared to the remaining sections of core ST5 (Fig. 6). The sediments in the south-west Aegean Sea and the Cretan Sea display a significant increase in illite and total clay mineral contents and, to a lesser degree, of smectite and kaolinite in the S1a and S1b horizons (Leontopoulou *et al.*, 2019).

The greater chlorite contents in the south-east Aegean Sea are attributed principally to supply from the widespread occurrences of basic/ultrabasic rocks in the mainland of west Turkey and, to a lesser degree, in the surrounding islands (Aksu *et al.*, 1995a; Ergin, 2012). Illite is the second most abundant mineral in core ST5 (average 7.8% wt.%), displaying lower abundances compared to the south-west Aegean Sea and the Cretan Sea (average 10.6 and 8.3 wt.%, respectively). Smectite is also present generally in lesser amounts in core ST5 (average 3 wt.%) compared to the south-west Aegean Sea and the Cretan Sea (3.8 wt.% on average in both cores). Therefore, there is a decrease in the illite and smectite contents in the south-east Aegean Sea sediments compared to their counterparts from the Cretan Sea and the south-west Aegean Sea. Similarly, the average kaolinite content is slightly lower in core ST5 (average 5.1 wt.%) compared to the south-west Aegean Sea and the Cretan Sea (average 5.4 and 5.7 wt.%, respectively) (Leontopoulou *et al.*, 2019). The presence of palygorskite is indicative of aeolian input in the Aegean, although terrestrial input might also be possible (Chamley, 1989), considering that the broader area of west Anatolia is characterized by alkaline,

Table 2. Correlation coefficient (Pearson's *r*) matrix of the major and trace elements in core ST5. Numbers in bold indicate *r* values >0.7.

	SiO ₂	TiO ₂	Al ₂ O ₃	Fe ₂ O ₃	MnO	MgO	CaO	Na ₂ O	K ₂ O	P ₂ O ₅	LOI	V	Cr	Co	Ni	Cu	Zn	Rb	Sr	Y	Zr	Ba	La	Ce	Nd	Pb	Th
SiO ₂	1	0.745	0.807	0.639	-0.088	-0.151	-0.585	0.686	0.807	0.359	-0.806	0.320	-0.262	0.392	0.223	0.354	0.824	0.792	-0.693	0.581	0.544	0.247	0.472	0.118	0.196	0.381	0.226
TiO ₂	0.745	1	0.798	0.241	0.301	-0.528	-0.311	0.374	0.742	0.361	-0.520	0.090	-0.457	0.017	-0.356	0.233	0.638	0.736	-0.710	0.673	0.749	-0.038	0.647	0.472	0.459	0.634	0.467
Al ₂ O ₃	0.807	0.798	1	0.677	0.107	-0.578	-0.651	0.336	0.982	0.574	-0.552	0.401	-0.732	0.246	-0.076	0.600	0.903	0.966	-0.700	0.811	0.423	0.300	0.543	0.228	0.408	0.470	0.473
Fe ₂ O ₃	0.639	0.241	0.677	1	-0.346	-0.120	-0.660	0.292	0.714	0.553	-0.629	0.625	-0.435	0.529	0.503	0.666	0.785	0.707	-0.365	0.600	-0.051	0.610	0.128	-0.196	0.024	-0.022	0.093
MnO	-0.088	0.301	0.107	-0.346	1	-0.480	0.358	-0.136	0.032	0.179	0.077	-0.164	-0.300	-0.275	-0.588	0.069	-0.039	0.023	0.038	0.212	0.283	-0.189	0.279	0.541	0.243	0.399	0.262
MgO	-0.151	-0.528	-0.578	-0.120	-0.480	1	0.108	-0.032	-0.554	-0.567	0.016	-0.126	0.841	0.329	0.748	-0.424	-0.424	-0.524	0.292	-0.618	-0.249	-0.090	-0.364	-0.513	-0.578	-0.635	-0.390
CaO	-0.585	-0.311	-0.651	-0.660	0.358	0.108	1	-0.255	-0.691	-0.086	0.170	-0.363	0.418	-0.517	-0.412	-0.308	-0.662	-0.719	0.728	-0.302	0.018	-0.304	-0.047	0.297	0.072	0.034	-0.208
Na ₂ O	0.686	0.374	0.336	0.292	-0.136	-0.032	-0.255	1	0.366	0.096	-0.588	0.081	0.048	0.163	0.107	0.026	0.438	0.293	-0.388	0.152	0.402	0.067	0.209	0.039	0.162	0.445	-0.063
K ₂ O	0.807	0.742	0.982	0.714	0.032	-0.554	-0.691	0.366	1	0.543	-0.566	0.446	-0.733	0.254	-0.014	0.612	0.925	0.980	-0.689	0.799	0.324	0.376	0.509	0.209	0.396	0.420	0.410
P ₂ O ₅	0.359	0.361	0.574	0.553	0.179	-0.567	-0.086	0.096	0.543	1	-0.466	0.589	-0.625	0.157	-0.160	0.661	0.613	0.531	-0.140	0.642	0.068	0.575	0.295	0.205	0.365	0.318	0.160
LOI	-0.806	-0.520	-0.552	-0.629	0.077	0.016	0.170	-0.588	-0.566	-0.466	1	-0.391	0.100	-0.273	-0.293	-0.456	-0.663	-0.535	0.276	-0.606	-0.408	-0.407	-0.385	-0.174	-0.157	-0.213	-0.059
V	0.320	0.090	0.401	0.625	-0.164	-0.126	-0.363	0.081	0.446	0.589	-0.391	1	-0.345	0.356	0.338	0.700	0.638	0.437	-0.254	0.454	-0.264	0.825	-0.065	0.028	-0.064	-0.060	-0.066
Cr	-0.262	-0.457	-0.732	-0.435	-0.300	0.841	0.418	0.048	-0.733	-0.625	0.100	-0.345	1	0.040	0.386	-0.589	-0.599	-0.716	0.350	-0.674	-0.029	-0.276	-0.381	-0.283	-0.495	-0.370	-0.477
Co	0.392	0.017	0.246	0.529	-0.275	0.329	-0.517	0.163	0.254	0.157	-0.273	0.356	0.040	1	0.647	0.239	0.391	0.308	-0.315	-0.024	-0.187	0.407	-0.160	-0.292	-0.213	-0.256	-0.067
Ni	0.223	-0.356	-0.076	0.503	-0.588	0.748	-0.412	0.107	-0.014	-0.160	-0.293	0.338	0.386	0.647	1	0.090	0.156	0.029	-0.024	-0.174	-0.381	0.424	-0.333	-0.597	-0.517	-0.635	-0.285
Cu	0.354	0.233	0.600	0.666	0.069	-0.424	-0.308	0.026	0.612	0.661	-0.456	0.700	-0.589	0.239	0.090	1	0.700	0.594	-0.198	0.735	-0.046	0.695	-0.040	0.188	0.067	0.041	0.333
Zn	0.824	0.638	0.903	0.785	-0.039	-0.424	-0.662	0.438	0.925	0.613	-0.663	0.638	-0.599	0.391	0.156	0.700	1	0.923	-0.672	0.741	0.233	0.608	0.364	0.130	0.269	0.301	0.256
Rb	0.792	0.736	0.966	0.707	0.023	-0.524	-0.719	0.293	0.980	0.531	-0.535	0.437	-0.716	0.308	0.029	0.594	0.923	1	-0.715	0.770	0.278	0.396	0.467	0.168	0.345	0.344	0.393
Sr	-0.693	-0.710	-0.700	-0.365	0.038	0.292	0.728	-0.388	-0.689	-0.140	0.276	-0.254	0.350	-0.315	-0.024	-0.198	-0.672	-0.715	1	-0.458	-0.399	-0.131	-0.252	-0.127	-0.100	-0.362	-0.295
Y	0.581	0.673	0.811	0.600	0.212	-0.618	-0.302	0.152	0.799	0.642	-0.606	0.454	-0.674	-0.024	-0.174	0.735	0.741	0.770	-0.458	1	0.372	0.389	0.410	0.450	0.334	0.431	0.459
Zr	0.544	0.749	0.423	-0.051	0.283	-0.249	0.018	0.402	0.324	0.068	-0.408	-0.264	-0.029	-0.187	-0.381	-0.046	0.233	0.278	-0.399	0.372	1	-0.387	0.452	0.381	0.237	0.607	0.454
Ba	0.247	-0.038	0.300	0.610	-0.189	-0.090	-0.304	0.067	0.376	0.575	-0.407	0.825	-0.276	0.407	0.424	0.695	0.608	0.396	-0.131	0.389	-0.387	1	-0.213	-0.088	-0.048	-0.216	-0.105
La	0.472	0.647	0.543	0.128	0.279	-0.364	-0.047	0.209	0.509	0.295	-0.385	-0.065	-0.381	-0.160	-0.333	-0.040	0.364	0.467	-0.252	0.410	0.452	-0.213	1	0.320	0.635	0.502	0.126
Ce	0.118	0.472	0.228	-0.196	0.541	-0.513	0.297	0.039	0.209	0.205	-0.174	0.028	-0.283	-0.292	-0.597	0.188	0.130	0.168	-0.127	0.450	0.381	-0.088	0.320	1	0.489	0.544	0.201
Nd	0.196	0.459	0.408	0.024	0.243	-0.578	0.072	0.162	0.396	0.365	-0.157	-0.064	-0.495	-0.213	-0.517	0.067	0.269	0.345	-0.100	0.334	0.237	-0.048	0.635	0.489	1	0.523	-0.008
Pb	0.381	0.634	0.470	-0.022	0.399	-0.635	0.034	0.445	0.420	0.318	-0.213	-0.060	-0.370	-0.256	-0.635	0.041	0.301	0.344	-0.362	0.431	0.607	-0.216	0.502	0.544	0.523	1	0.322
Th	0.226	0.467	0.473	0.093	0.262	-0.390	-0.208	-0.063	0.410	0.160	-0.059	-0.066	-0.477	-0.067	-0.285	0.333	0.256	0.393	-0.295	0.459	0.454	-0.105	0.126	0.201	-0.008	0.322	1

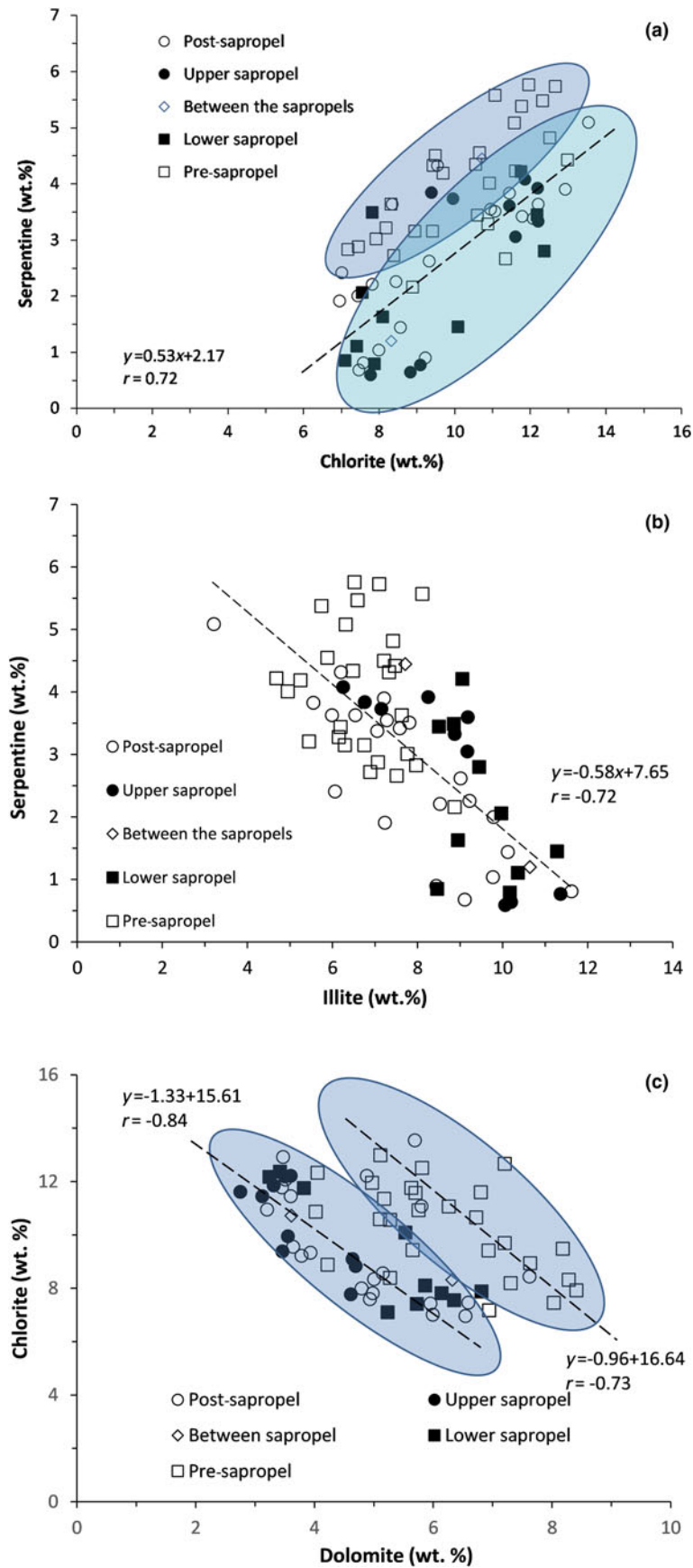


Fig. 4. (a) Serpentine vs chlorite, (b) serpentine vs illite and (c) chlorite vs dolomite in the ST5 sediments. The two shaded areas indicate the two groups of samples displaying subparallel trends. See text for discussion.

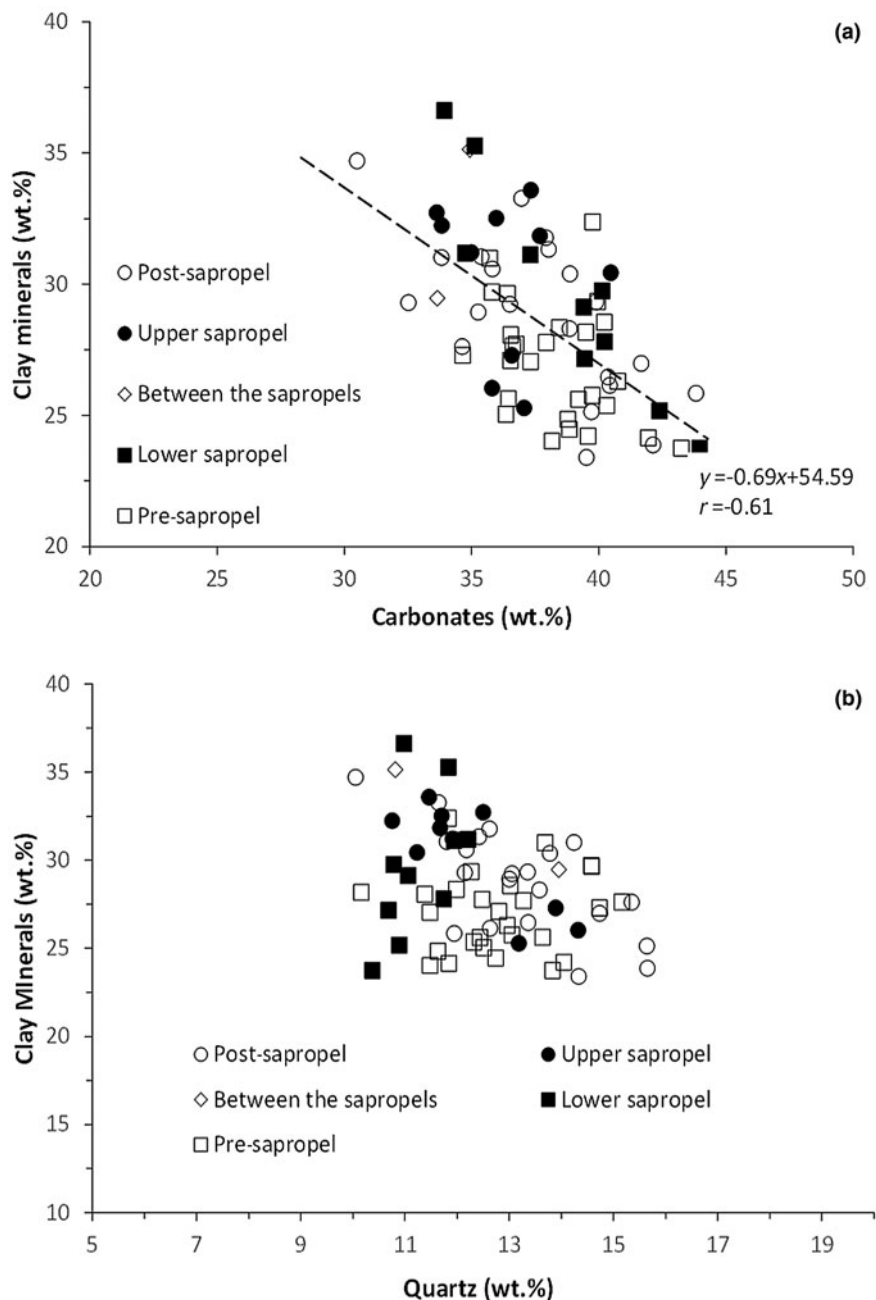


Fig. 5. Clay minerals vs (a) total carbonates and (b) quartz.

palygorskite-bearing soils (Kadir *et al.*, 2014). The palygorskite content in core ST5 (average 2 wt.%) is slightly smaller than those of the Cretan Sea (average 2.4 wt.%) and the south-west Aegean Sea (average 2.2 wt.%). Although several of the differences in the average abundances of clay minerals are within the uncertainty bounds of the analytical method, they refer to average values over large sets of samples in each core, suggesting that they are statistically significant.

Slight increases in the illite and total clay contents are also observed in core ST5, which are less pronounced compared to in the south-west Aegean Sea and the Cretan Sea (e.g. compare Fig. 6 & Table S1 with Leontopoulou *et al.*, 2019). By contrast, in core ST5 the smectite content increases gradually from the base of the sapropel horizon upwards, without particular enrichment in the sapropel horizon (Fig. 6). Finally, the illite/kaolinite

(I/K) and smectite/kaolinite (S/K) ratios increase gradually towards the top (Fig. 7), a trend that is more apparent for the S/K ratio. The illite/chlorite and chlorite/kaolinite ratios do not display any particular trends with depth (data not shown).

After heating of the clay fractions at 530°C and subsequent EG solvation the smectite remained essentially unaffected, as is indicated by the position of the 001 diffraction maximum at ~17 Å, although the intensity of the maximum decreased, especially in the pre-sapropel sediments (Fig. S2). This feature suggests that a significant fraction of the smectite has a high dehydroxylation temperature, indicating a *cis*-vacant octahedral occupancy (Drits *et al.*, 1998). The decrease in intensity of the 001 maximum, especially in the pre-sapropel sediments, indicates that *trans*-vacant smectite might also be present, which may predominate in the pre-sapropel sediments. In comparison, the smectites in the

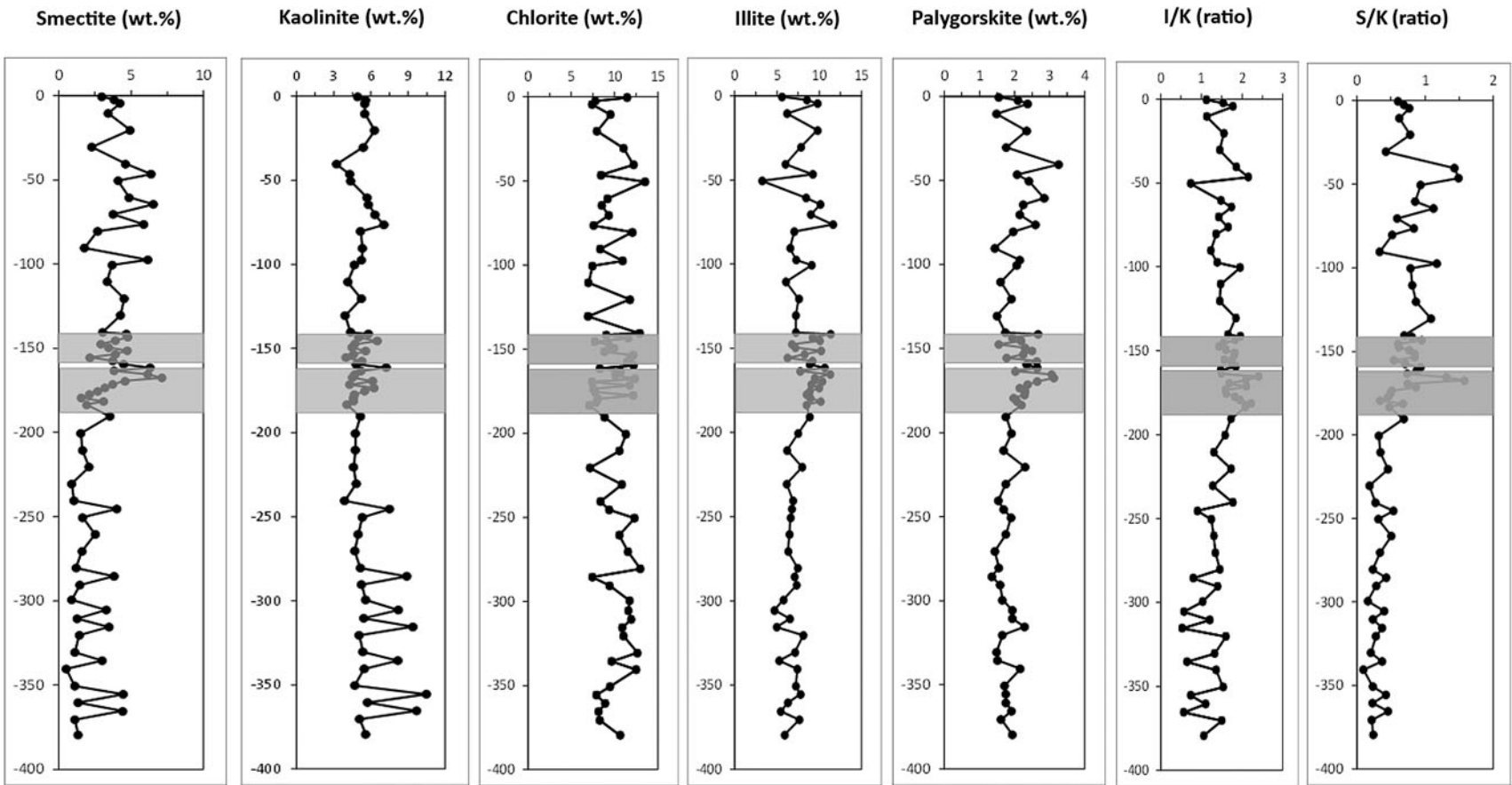


Fig. 6. Downcore variation of clay minerals (wt.%) and I/K and S/K ratios in core ST5 determined using the Rietveld method. The shaded areas indicate sapropel S1. The vertical axes denote the depth bsf.

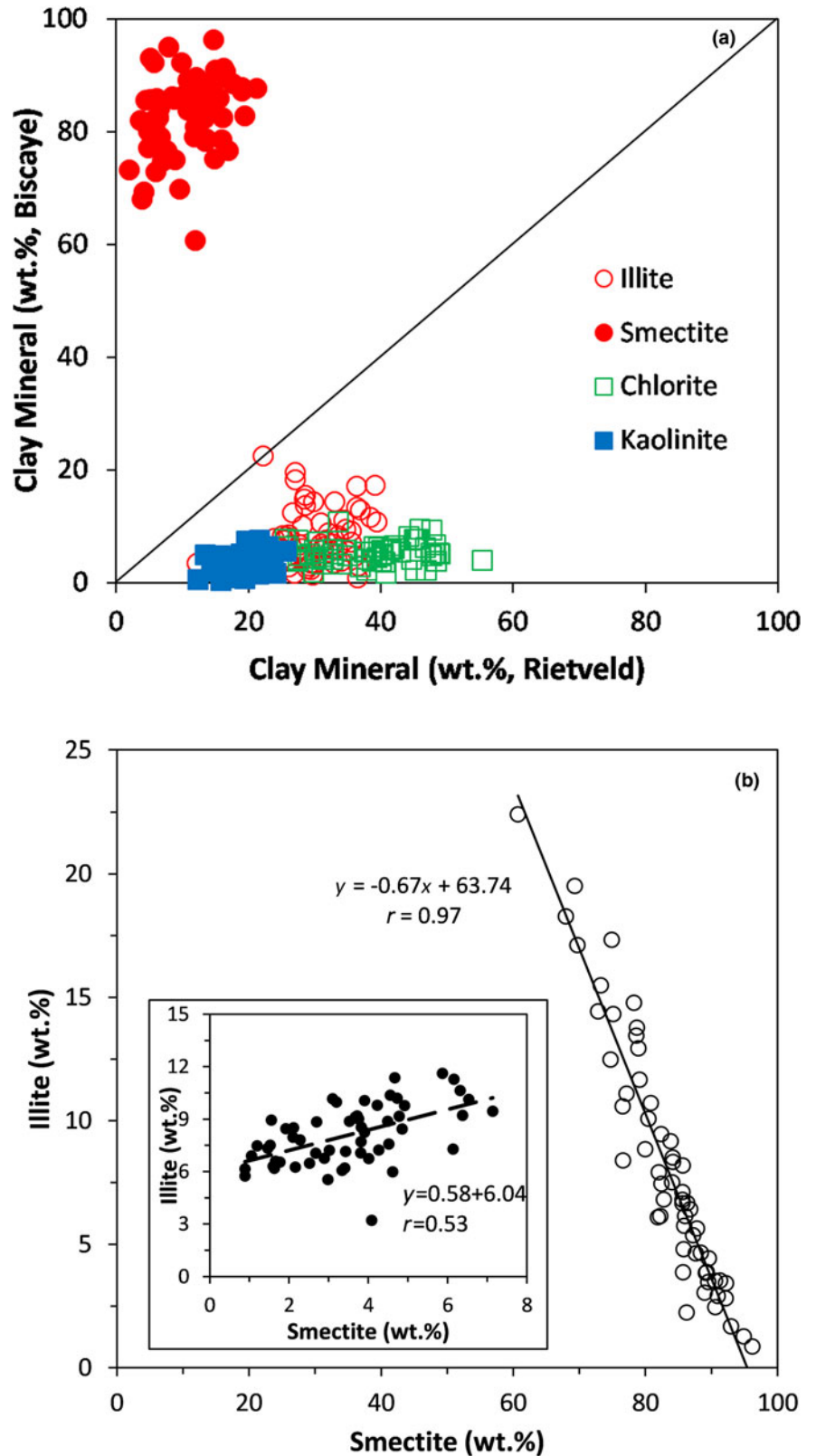


Fig. 7. (a) Correlation between the clay mineral contents determined using Rietveld refinement of the bulk sediments and the method of Biscaye (1965) in the clay fractions. (b) Smectite vs illite trends obtained from the Biscaye method (open circles) and the Rietveld method (inset). See text for discussion.

Cretan Sea displayed *cis*-vacant behaviour, whereas the smectites in the south-west Aegean Sea displayed *trans*-vacant behaviour characterized by low dehydroxylation temperatures (Leontopoulou *et al.*, 2019). In the clay fraction, abundant serpentine occurred as an additional 7 Å phase, as well as kaolinite, chlorite, carbonates

(mainly calcite and Mg-calcite) and quartz, while traces of palygorskite were detected only in a few samples. Dolomite occurred mainly in the silt and sand fractions.

The abundances of the four clay minerals determined using the Rietveld method normalized to 100% and their counterparts

determined using the method proposed by Biscaye (1965) are listed in Table S3. A comparison of the abundances of the individual clay minerals determined using the two methods clearly indicates an underestimation of smectite and an overestimation of the remaining clay minerals in the former approach compared to the latter (Fig. 7a). A similar trend was observed in the south-west Aegean Sea and the Cretan Sea, except for the fact that the illite content was comparable when using the two methods (Leontopoulou *et al.*, 2019). As a portion of the chlorite and illite (mica) crystals will be coarser than 2 μm , the use of only the clay fraction is not reliable for complete palaeogeographical and/or palaeoclimatic interpretations and does not provide complete information about weathering mechanisms in the source areas. The overestimation of smectite when using the method proposed by Biscaye (1965) is due to the fine particle size of smectite crystallites that settle after the remaining clay minerals, causing a 'smearing effect' (Leontopoulou *et al.*, 2019). This is a potential reason as to why minor clay minerals such as palygorskite may not be identified in oriented mounts. The striking difference in the trend for illite underlines the influence of particle size on the quantitative determination of phyllosilicates using the various methods, and its ramifications for the sedimentation regime are addressed in the 'Discussion' section. In addition, the two methods yielded different trends between clay minerals. The Rietveld method yielded a weak positive correlation between smectite and illite ($r=0.53$), whereas the method proposed by Biscaye yielded a very strong negative correlation between the two minerals ($r=-0.97$; Fig. 7b). Similar trends were reported by for the south-west Aegean Sea and the Cretan Sea (Leontopoulou *et al.*, 2019).

Examination of the clay fractions using SEM demonstrated the presence of *Emiliania huxleyi* coccolithophore fragments and clay minerals (Fig. S3). In addition, fine-grained, well-crystallized calcite is present in most samples. Calcite is associated locally with pyrite. No dolomite was identified in the SEM micrographs, which is in accordance with the XRD results. The EDS analyses of the clay minerals demonstrated the presence of mixtures of illite, smectite and chlorite. It was not possible to isolate crystals of individual clay minerals. *Emiliania huxleyi* is generally a main coccolithophore in the lower and upper euphotic zones of the Mediterranean. It predominates in the surface waters of the Aegean Sea, mainly in winter/spring, and it indicates greater values of S and the beginning of a nutrient-rich euphotic zone (Triantaphyllou *et al.*, 2009). In general, the abundance of coccolithophores decreases with depth. Moreover, the sapropel sediments display a significant decrease in coccolithophores, which is in accordance with the reduction in the CaO content in the geochemical analysis compared to the pre- and post-sapropel sediments.

Geochemistry of core ST5

Major elements. The downcore distribution of major elements is shown in Fig. 8a, while the geochemical data are listed in Table S4. The abundances of SiO_2 , Al_2O_3 , Fe_2O_3 , Na_2O and K_2O increase gradually upcore, decreasing in the uppermost 40 cm. Moreover, with the exception of Na_2O , the sapropel S1 horizon is enriched in these elements compared to the sediments immediately before and after the sapropel. By contrast, MgO displays the opposite trend, decreasing gradually upcore. Again, the sapropel S1 horizon is enriched in MgO compared to the pre- and post-sapropel sediments. Finally, CaO does not display a clear

overall trend throughout the core. Nevertheless, it decreases in post-sapropelic sediments up to 40 cm bsf, increasing thereafter. The CaO contents of the samples were calculated independently of the abundances of calcite, Mg-calcite, aragonite and dolomite using the end-member compositions for calcite, aragonite and dolomite and considering the 10% Mg mole in Mg-calcite. The calculated CaO contents were within $\pm 5\%$ (relative error) of the CaO contents determined using XRF spectroscopy, suggesting that the carbonate abundances determined by the quantitative analysis are reliable. Considering that SiO_2 , Al_2O_3 , Fe_2O_3 and Na_2O are associated with the clastic component and CaO is associated mainly with the authigenic carbonate component in the sediments, it is evident that in post-sapropelic sediments the clastic component increases upwards up to 40 cm bsf and that the authigenic component increases in abundance in the uppermost layers.

The sediments in core ST5 have, on average, greater SiO_2 , MgO, Fe_2O_3 , and TiO_2 contents and smaller CaO, Al_2O_3 , Na_2O and K_2O contents compared to their counterparts in the south-west Aegean Sea and the Cretan Sea (compare Fig. 8a and Table S4 with data in Leontopoulou *et al.*, 2019). The elemental composition is in accordance with the mineralogical composition of the sediments, confirming the reliability of the quantitative mineralogical analysis. Thus, the greater SiO_2 and Fe_2O_3 contents are due to the greater quartz and total clay mineral abundances. The greater MgO content in core ST5 compared to those of the south-west Aegean Sea and Cretan Sea sediments is due to the greater chlorite, serpentine and dolomite contents in the former, because the Mg-calcite content is smaller in core ST5 compared to sediments in the south-west Aegean Sea and the Cretan Sea. The overall large CaO contents are related to the abundance of carbonates in the sediments (Fig. 8a). The smaller CaO content in core ST5 sediments than their counterparts in the south-west Aegean Sea and the Cretan Sea is in accordance with a smaller carbonate content in the former. Similarly, the smaller Na_2O and K_2O contents in core ST5 are in full accordance with the smaller feldspar and illite contents when compared to those of the south-west Aegean Sea and Cretan Sea sediments.

The Chemical Index of Alteration (CIA) values of the sediments (Nesbitt & Young, 1982), are shown in Fig. 8a. The CaO content was omitted from the calculations because of the large abundance of carbonates in the samples. The CIA has been used as an efficient indicator of the intensity of weathering and subsequently as a palaeoclimatic proxy (Nesbitt & Young, 1982; Meunier *et al.*, 2013). The CIA ranges from 70 to 76 in core ST5 and averages ~ 73 (Fig. 9a). Such values are comparable with the average shale composition (Nesbitt & Young, 1982) and are greater than the corresponding values for the south-west Aegean Sea and Cretan Sea sediments. In addition, the CIA displays a slight, gradual increase with decreasing depth (Fig. 8a). When MgO was included in the calculation of the CIA, after correction for the Mg present in Mg-calcite and dolomite, the $\text{CIA}_{(\text{Mg})}$ index displayed a well-defined increase with decreasing depth (Fig. 8a). The sapropel S1 sediments have greater $\text{CIA}_{(\text{Mg})}$ indices than their counterparts in pre- and post-sapropel S1 sediments.

The $\text{Al}_2\text{O}_3/\text{TiO}_2$ ratio of the sediments in core ST5 varies between 13.8 and 19.2 with an average value of 17.2 (Fig. 8a), being smaller than those reported in the south-west Aegean Sea (average $\text{Al}_2\text{O}_3/\text{TiO}_2$ ratio = 21.1) and Cretan Sea sediments (average $\text{Al}_2\text{O}_3/\text{TiO}_2$ ratio = 19.1) (Leontopoulou *et al.*, 2019). The sediments of sapropel S1 have greater ratios than their in

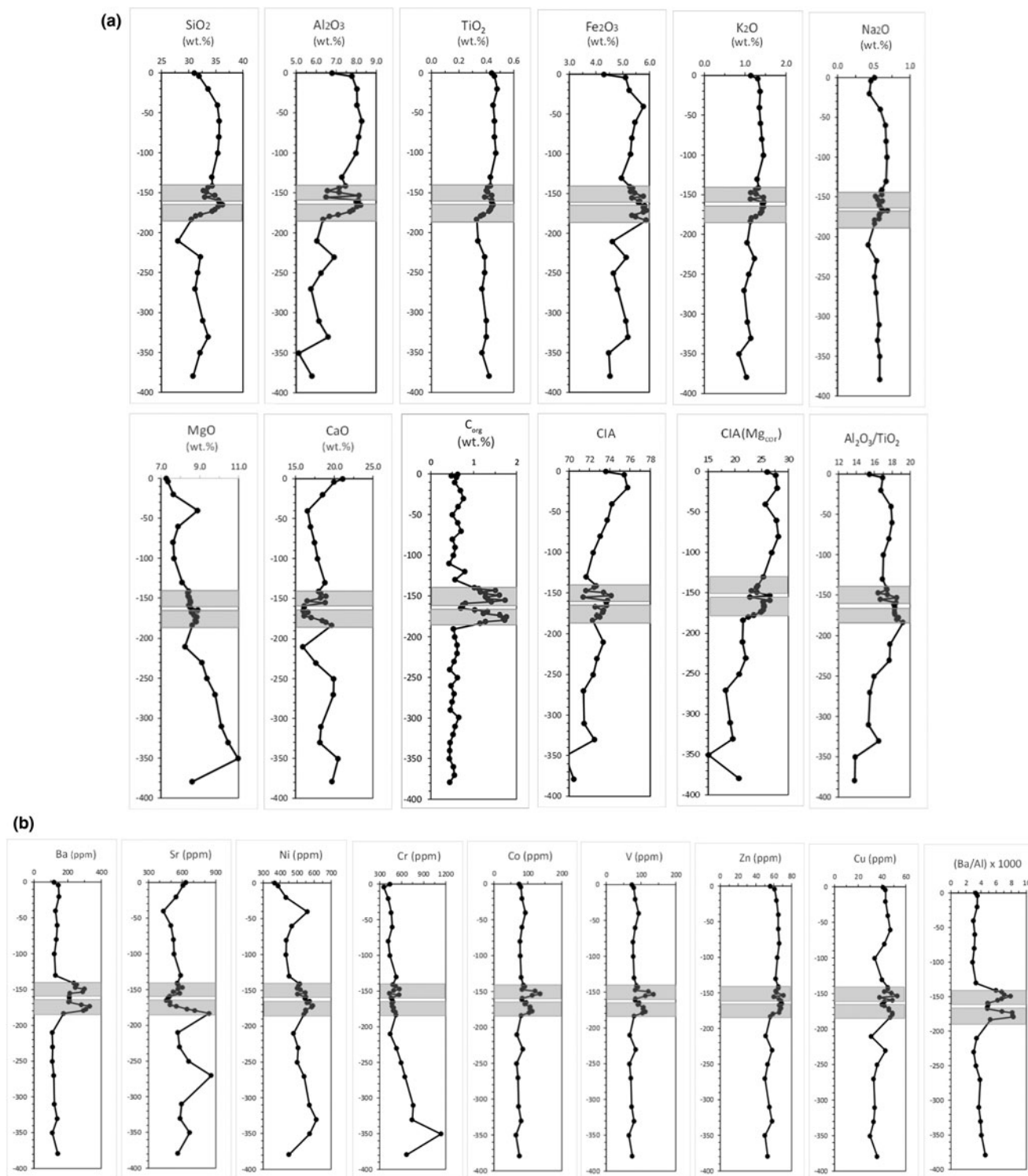


Fig. 8. Downcore variation of (a) major elements and (b) trace elements along core ST5. The shaded areas indicate sapropel S1. The vertical axes denote the depth bsf.

pre- and post-sapropel S1 counterparts. The $\text{Al}_2\text{O}_3/\text{TiO}_2$ ratio is frequently used as a palaeoclimatic proxy (Kiipli *et al.*, 2012). Values <20 are typically considered to be indicative of a humid climate and those between 20 and 30 are typically considered to be indicative of semi-humid/semi-arid climates in the sediment source areas. Large Ti/Al ratios have been used as a proxy for

increasing aeolian input in recent Central Mediterranean sediments (Bout-Roumazeilles *et al.*, 2013).

Trace elements. Ba, Ni, Co and V are enriched in the sapropel S1 sediments compared to the remaining core sediments (Fig. 8b). Barium in marine sediments is typically hosted in marine barite (BaSO_4) and is associated with organic matter (Karageorgis

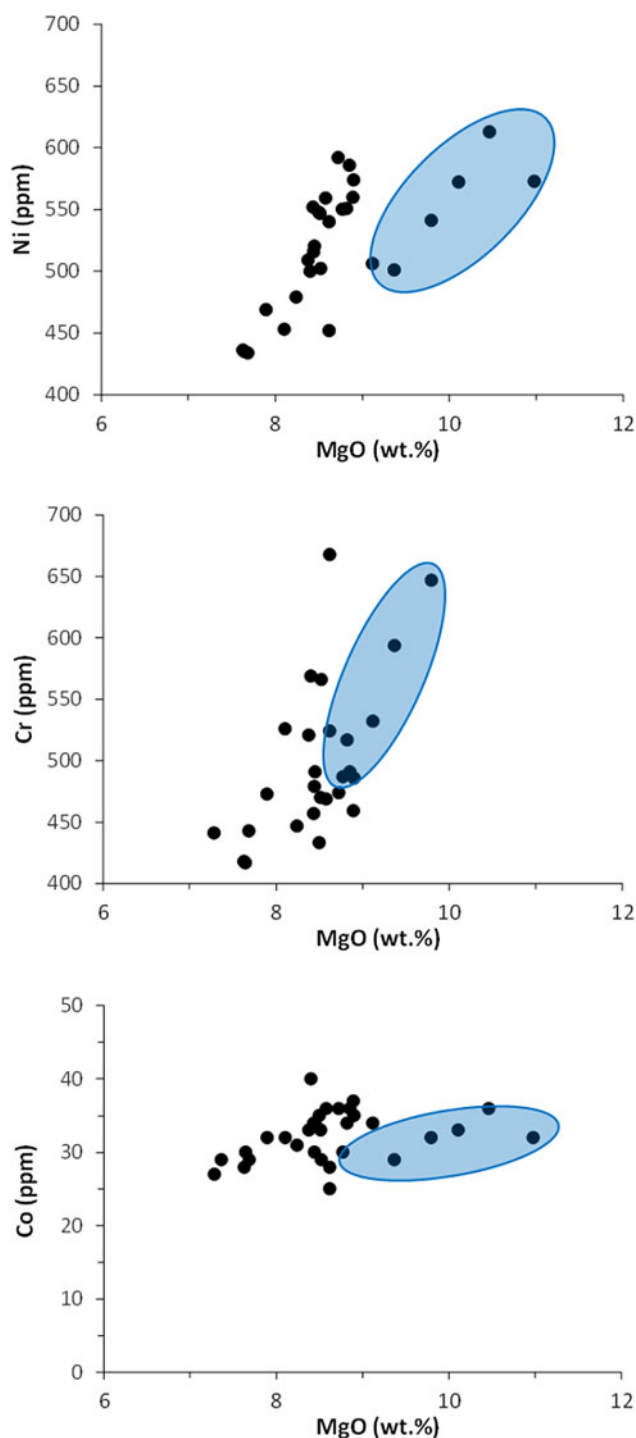


Fig. 9. MgO vs Ni, Cr and Co. The shaded areas indicate samples from the lowermost section of the core.

et al., 2005). All sapropel sediments are enriched in Ba, as is indicated by the Ba/Al ratio (Fig. 8b). Increased contents of Ba in sediments rich in organic matter are considered to represent a reliable palaeoproductivity proxy for this environment (Van Santvoort *et al.*, 1996; Thomson *et al.*, 1999; Martinez-Ruiz *et al.*, 2000; Filippidi *et al.*, 2016). The abundances of Zn and Cu increase from the bottom of sapropel S1 upwards, being lower in the pre-sapropelic sediments. Cr and Ni decrease gradually upwards following the distribution of MgO (Fig. 8a).

Indeed, MgO shows clear positive trends with Cr, Ni and Co (Fig. 9). Samples from the lowermost section of the core follow a different linear trend characterized by greater MgO contents (Fig. 9). By contrast, Zn and Rb and, to a lesser degree, Cu (Fig. 8b) follow the opposite trend, increasing upwards (i.e. they display similar distributions to SiO₂, Al₂O₃, Fe₂O₃, Na₂O and K₂O; Fig. 8a). The trend for Cu may reflect the lower precision of the analytical method at low concentrations of Cu (Georgakopoulou *et al.*, 2017).

The Pearson correlation coefficients (r) between major and trace elements are listed in Table 2. Pearson's correlation coefficient values >0.7 indicate very good correlations and are highlighted in bold. The chemical elements that display very good correlation can be separated into three different groups, indicating at least two distinct clastic sources and certain geochemical/mineralogical processes. The first group, indicating a clastic source, includes incompatible elements of crustal affinities (SiO₂, Al₂O₃, TiO₂, K₂O, Rb, Zn, Y, Zr, Sr, Cu); the second clastic group comprises compatible elements of mantle affinities (Mg, Co, Ni, Cr); and the third group includes elements related to certain geochemical/mineralogical processes and includes Ca, Sr, Ba and V. Ca and Sr are related at least partly to the carbonate component in the sediments, both biogenic and clastic, while Ba and V are associated with the C_{org} being enriched in the sapropel S1 horizon.

Organic carbon. The C_{org} content in core ST5 varies considerably and ranges from 0.44 to 1.73 wt.% (Fig. 8a), with the maximum values occurring in the sapropel S1 interval where the C_{org} content exceeds 1 wt.%. The lower unit (S1a) and the upper unit (S1b) of the sapropel S1 sequence are characterized by a maximum C_{org} content of 1.77 wt.% and average contents of 1.30 and 1.34 wt.%, respectively. Both the maximum C_{org} value and the greatest Ba/Al ratio were recorded at a depth of 179.5 cm in a sample from the S1a layer. Generally, increased abundances of C_{org} are accompanied by similar increases in hydrogen and nitrogen content (data not shown). During the interruption of the sapropel S1 sequence, the C_{org} content decreases markedly to 0.74 wt.%, but this is still greater than in the pre-sapropel levels.

Chronostratigraphy and sedimentation rates in core ST5

The calibrated ¹⁴C radiometric ages obtained at 41.0, 100.0, 180.5 and 255.0 cm were 2086 ± 30, 4562 ± 30, 8900 ± 30 and 16,912 ± 30 years BP, respectively (Fig. 2). The apparent sedimentation rates calculated were 19.7 cm ka⁻¹ at the first and uppermost interval, 23.8 cm ka⁻¹ at the second interval, 18.6 cm ka⁻¹ at the third interval and 9.3 cm ka⁻¹ at the last interval. The depth of 180.5 cm corresponds to the base of the S1a sapropel bed (Fig. 2). The average sedimentation rate for the interval represented by the core is 17.3 cm ka⁻¹, which is significantly greater than the sedimentation rates in the Myrtoon Basin (south-west Aegean Sea) and the Cretan Sea, where the rates were 10.2 and 4.7 cm ka⁻¹, respectively (Leontopoulou *et al.*, 2019).

Discussion

Comparison with the cores in the north-west and south Aegean

Core ST5 displays sedimentological, mineralogical and geochemical differences from cores C40 and TI13 from the south-west and south Aegean Sea, respectively (Leontopoulou *et al.*, 2019). These differences are associated with provenance areas and regional

current circulation patterns. Core ST5 is characterized by considerably greater sedimentation rates and displays an apparent inconsistency: although the sediments are considerably richer in the clay fraction and poorer in the sand fraction than their counterparts from cores C40 and T113, the average D_{50} of core ST5 is greater than the average D_{50} of core T113. This apparent inconsistency is explained by the coarser particle size in core ST5 compared to core T113, a probable consequence of the vicinity of the core to the west Anatolian landmass.

In addition to the overestimation of the smectite relative to the remaining clay minerals when using the method of Biscaye (1965), which is a general observation for sediments throughout the south Aegean Sea, the sediments of core ST5 are characterized by two features distinguishing them from other Aegean sediments (cf. Leontopoulou *et al.*, 2019): (1) the presence of chlorite as the dominant clay mineral and the abundance of serpentine; and (2) underestimation of illite in addition to kaolinite and chlorite when using the method of Biscaye (1965) (Fig. 7a). This suggests the sediment is supplied by mainly basic/ultrabasic source rocks and the occurrence of illite along with kaolinite and chlorite mainly in the silt fraction of the sediments. In addition, sorting has a limited influence on the distribution of clay minerals in the sediments of core ST5, as indicated by the lack of particular trends between either quartz and clay minerals (Fig. 5b) or quartz and the I/K (data not shown). This is in contrast to the sediments from the south-west Aegean Sea and the Cretan Sea, which displayed evidence for the influence of sorting in the clay mineral composition (Leontopoulou *et al.*, 2019). This suggests that all clay minerals except for smectite, along with quartz, participate in the silt fraction of the core ST5 sediments, indicating limited transportation of these sediments.

Furthermore, the sediments of core ST5 have greater MgO contents than their counterparts from cores C40 and T113 (Leontopoulou *et al.*, 2019), which is explained by the presence of chlorite, dolomite and serpentine (Table 1). The MgO-bearing minerals are related to the predominance and provenance of the clastic component of the sediments. Indeed, although dolomite and Mg-calcite have comparable abundances in the bulk ST5 sediments (Table 1), the clay fractions are considerably enriched in Mg-calcite compared to dolomite based on the peak areas of these minerals. The latter mineral is absent or only present in trace amounts in the clay fractions. The presence of trace dolomite in the clay fractions compared to its abundance in the bulk sediments is indicative of a mainly clastic origin of this carbonate. The high sedimentation rate in core ST5 due to the supply of sediments from the nearby ophiolitic landmasses yielded abundant serpentine, amphibole and chlorite.

Previous work has suggested that the smectite in the south-east Aegean Sea sediments might have been supplied by rivers from the surrounding landmasses of Asia Minor (Aksu *et al.*, 1995b; Rousakis *et al.*, 2004; Ehrmann *et al.*, 2007; Ergin *et al.*, 2007, 2012; Poulos, 2009) with a significant/dominant contribution of Nile-derived sediments and sediments from south Turkey (Cilicia) (Venkatarathnam & Ryan, 1971; Ehrmann *et al.*, 2007, 2013; Poulos, 2009). The crystal chemical characteristics of smectite in core ST5 are similar to those of core T113 within the sapropel S1 and in the post-sapropel sediments, characterized by a high dehydroxylation temperature typical of *cis*-vacant octahedral sheets (Drits *et al.*, 1998). Such smectites with low octahedral Fe contents and low tetrahedral charges are not of pedogenic but usually of volcanogenic origin, being present in bentonites formed from the alteration of acidic-intermediate volcanoclastic

rocks. The smectites in pre-sapropel sediments contain both *cis*-vacant and *trans*-vacant smectites (Fig. S1). By contrast, alteration of basic volcanoclastic rocks yields *trans*-vacant smectites (Christidis 2006; Fontaine *et al.*, 2020). In addition, pedogenic smectites are usually Fe-montmorillonites and Fe-rich beidellites (Wilson, 1999). Such smectites have been described in sediments from the Nile River, the Cilicia Basin and north of Cyprus, in soils from the Ceyhan region of south Turkey, in the Cypriot bentonites and in vertisols in Turkey (Weir *et al.*, 1975; Shaw & Bush, 1978; Özkan & Ross, 1979; Güzel & Wilson, 1981; Christidis, 2006), being common in soils. In this sense, the decrease in the intensity of the 001 maximum of smectite in the pre-sapropel sediments after heating (Fig. S1) might indicate the coexistence of pedogenic smectite.

The formation of smectites in soils is controlled by low-lying topography, poor drainage and base-rich parent material (Borchardt, 1989). Thus, smectites are common in Mediterranean and temperate soils, which display limited leaching and are usually accompanied by illite (Thiry, 2000). Therefore, minor pedogenic smectite, if present, cannot be ascribed unequivocally to a specific source. However, certain mineralogical and geochemical trends in the sediments indicate that non-Aegean sources are unlikely to have contributed to the observed sedimentary patterns. This is discussed in the following section.

Implications for sedimentation patterns in the south-east Aegean Sea

The water circulation in the Aegean Sea is dominated by a general anticlockwise current of surface water, which consists of several small-scale eddies, the intensities and locations of which vary according to the seasonal wind field (Pinardi & Masetti, 2000; Lykousis *et al.*, 2002). Core ST5 was collected close to the area at which warm LSWs enters the Aegean Sea. Therefore, the proposed contribution of Nile and southern Turkey sediments that was mentioned previously (Venkatarathnam & Ryan, 1971; Ehrmann *et al.*, 2007, 2013; Poulos, 2009) would seem plausible.

However, there is ample evidence that the contribution of south-east Mediterranean sediments might not be significant in core ST5. Firstly, the core is characterized by a considerably greater sedimentation rate than the C40 and especially the T113 cores from the south-west Aegean Sea and the Cretan Sea, respectively. The high sedimentation rate is attributed to the close proximity of the studied core to the western Turkey landmass, which provides abundant terrestrial sedimentary load through the discharge of the Büyük Menderes River, its tributaries and the smaller Dayan and Dalaman rivers. In addition, sediment supply from the nearby islands of Rhodes, Simi and Tilos and the volcanic island of Nisyros contributed to the high sedimentation rates.

Secondly, the abundances of serpentine and chlorite in the ST5 sediments strongly indicate the presence of ultrabasic source rocks. The nearby landmass of western Turkey is characterized by large outcrops from the melanges (Marmaris ophiolite) in the Lycian nappes (Yilmaz & Yilmaz, 2013; Parlak, 2016; Güngör *et al.*, 2018). The presence of greater proportions of hornblende than in the C40 and T113 cores is also associated with the ophiolite rocks and it is attributed to weathering of amphibolites present in the Lycian nappes (Güngör *et al.*, 2018). Serpentine is a common hydrothermal alteration product of olivine (Deer *et al.*, 2013), which might also form during the alteration/lateritization

of ultrabasic rocks (Christidis & Mitsis, 2006; Villanova-de-Benavent *et al.*, 2017; Munoz *et al.*, 2019). However, recent lateritic profiles are absent in the Lycian ophiolites. This is in accordance with the temperate climate in the broader area, which was interrupted by humid periods, during the Uppermost Pleistocene and Holocene. Therefore, serpentine is likely to have originated from erosion of the Lycian ophiolites.

Thirdly, the geochemical signature of the ST5 sediments, characterized by high MgO, Cr, Ni and Co contents (Table 2) and the positive trends of MgO vs Ni, Cr and Co (Fig. 9), is in full accord with geochemical control by ophiolites of the Lycian nappes. Two trends are distinguished in the diagrams shown in Fig. 9. The pre-sapropel S1 sediments are characterized by greater MgO contents. When plotted on the Y/Ni vs Cr/Ni diagram used to trace the possible influence of ophiolite source rocks in the early Palaeozoic Taconic flysch (McLennan *et al.*, 1993), all sediments plot close to the 'ophiolite pole' (Fig. 10). When compared to the Taconic flysch samples, the ST5 sediments have very low Y/Ni ratios, suggesting a limited contribution of non-ophiolite components. In addition, the sapropel S1 samples display a nearly constant Y/Ni ratio, whereas the non-sapropel S1 sediments are characterized by greater variation in the Y/Ni ratio (see inset in Fig. 10). Moreover, the samples from the lowermost sections of the core have greater Cr/V ratios. Hence, the nearby landmasses were major sources of sediments in core ST5, suggesting only limited transportation of the clastic components. In addition, the ample supply of clastic sediments reduced chemical sedimentation, yielding lower Mg-calcite contents and low carbonate/clay mineral ratios throughout the core. By contrast, the riverine sediment supply from the Greek mainland is limited in the Myrtoon Basin (core C40) and in the Cretan Sea (core TI13), leading to greater calcite and Mg-calcite contents and greater carbonate/clay mineral ratios (Leontopoulou *et al.*, 2019). Finally, most of the smectites present have high dehydroxylation temperatures, being indicative of a volcanogenic origin (e.g. alteration of volcanic glass) rather than a pedogenic origin. Such smectites might have originated from erosion of the volcanoclastic rocks of Nisyros Island.

The contribution of aeolian material from the Sahara Desert is another component that might complicate provenance interpretations. In general, palygorskite has been used to indicate a Saharan origin of dust (Coudé-Gaussen *et al.*, 1982; Molinaroli, 1996; Caquineau *et al.*, 1998), although riverine input from the western Anatolia landmass might be an additional source (Chamley, 1989). Based on the data of Christidis *et al.* (2010), Leontopoulou *et al.* (2019) calculated that up to 50% of the kaolinite in cores C40 and TI13 might be attributed to Saharan dust. A similar kaolinite contribution from Saharan dust was calculated for core ST5 based on the data shown in Table 1, although the abundance of palygorskite was lower in core ST5 compared to cores C40 and TI13. The kaolinite content was also lower in core ST5 (Table 1). The main source of the remaining kaolinite probably originated from the nearby landmass, as the coastal sediments in the main river mouths in western Anatolia (e.g. Büyük Menderes, Dalyan, Dalaman) contain minor kaolinite (Bayhan *et al.*, 2001; Ehrmann *et al.*, 2007). However, the presence of abundant ophiolitic outcrops is not compatible with the formation of kaolinite during weathering due to the limited amount of Al present in ultrabasic rocks. Hence, pedogenic kaolinite is linked to weathering of the non-ophiolitic rocks of the Lycian nappes. By contrast, *trans*-vacant smectite in pre-sapropel sediments may form from weathering of ultrabasic rocks, and indeed

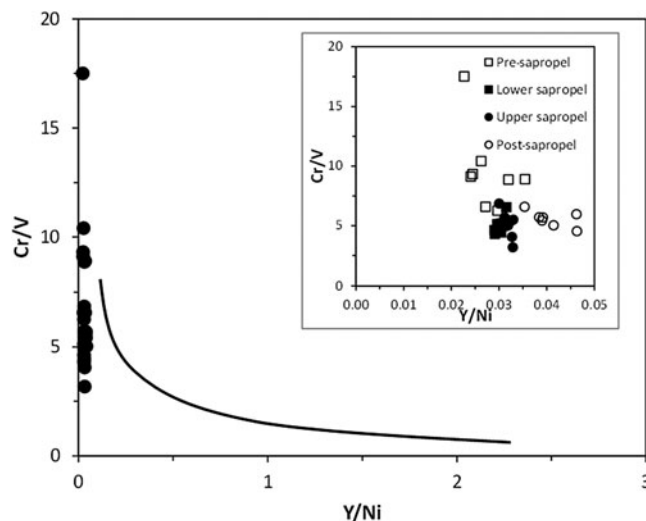


Fig. 10. Projection of the sediments in the Y/Ni vs Cr/V diagram (McLennan *et al.*, 1993). The inset is a magnification at the low Y/Ni ratio end. The curve indicates the trend of the Taconic flysch samples. See text for discussion.

Fe-rich smectites, containing minor octahedral Ni, are common weathering products of ultrabasic rocks (Decarreau *et al.*, 1987; Gaudin *et al.*, 2004; Christidis & Skarpelis, 2010; Mano *et al.*, 2014; Munoz *et al.*, 2019). Hence, Fe-smectite might also be a source of Ni, especially in the pre-sapropel sediments, reflecting the greater influence of the mantle component at these levels, as mentioned previously. Nevertheless, in general, serpentine and, to a lesser degree, talc are considered the major hosts of Ni. The increase in smectite content upcore is compatible with the greater participation of the crustal component and parallels the increase in abundance of the *cis*-vacant smectite.

Further implications of this study

The suggested circulation pattern in the area is shown schematically in Fig. 11. Although core ST5 is within the trajectory of the currents coming in the south-east Aegean Sea from the south-east Mediterranean Sea, the main source of these sediments is the landmass of western Anatolia. In this pattern, local source areas in the west Anatolian landmass control the mineralogical and geochemical composition of sediments in the south-east Aegean Sea. Furthermore, overall marine circulation patterns are of limited importance for the deposition of recent sediments in these areas. Although the Aegean Sea is a relatively closed basin and such sedimentation patterns might be expected, marine circulation was important for sedimentation in the south-west Aegean Sea and the Cretan Sea (Leontopoulou *et al.*, 2019). The greater influence of circulation patterns in the latter sites is attributed to the lack of significant riverine supply from the east Greek mainland and the Aegean Islands, including Crete. However, the role of local source areas in the composition of the sediments has been underestimated in previous studies. In addition, the reported well-defined clay mineral pattern characterized by large smectite/illite ratios in east and south Aegean sediments, due to the gradual increase in the smectite content towards the east (e.g. Ehrmann *et al.*, 2007) does not seem to be valid because the smectite content was smaller in core ST5 compared to that in core C40 (west Aegean Sea) and core TI13 (Cretan Sea). A significant contribution of Nilotic smectite would have increased the

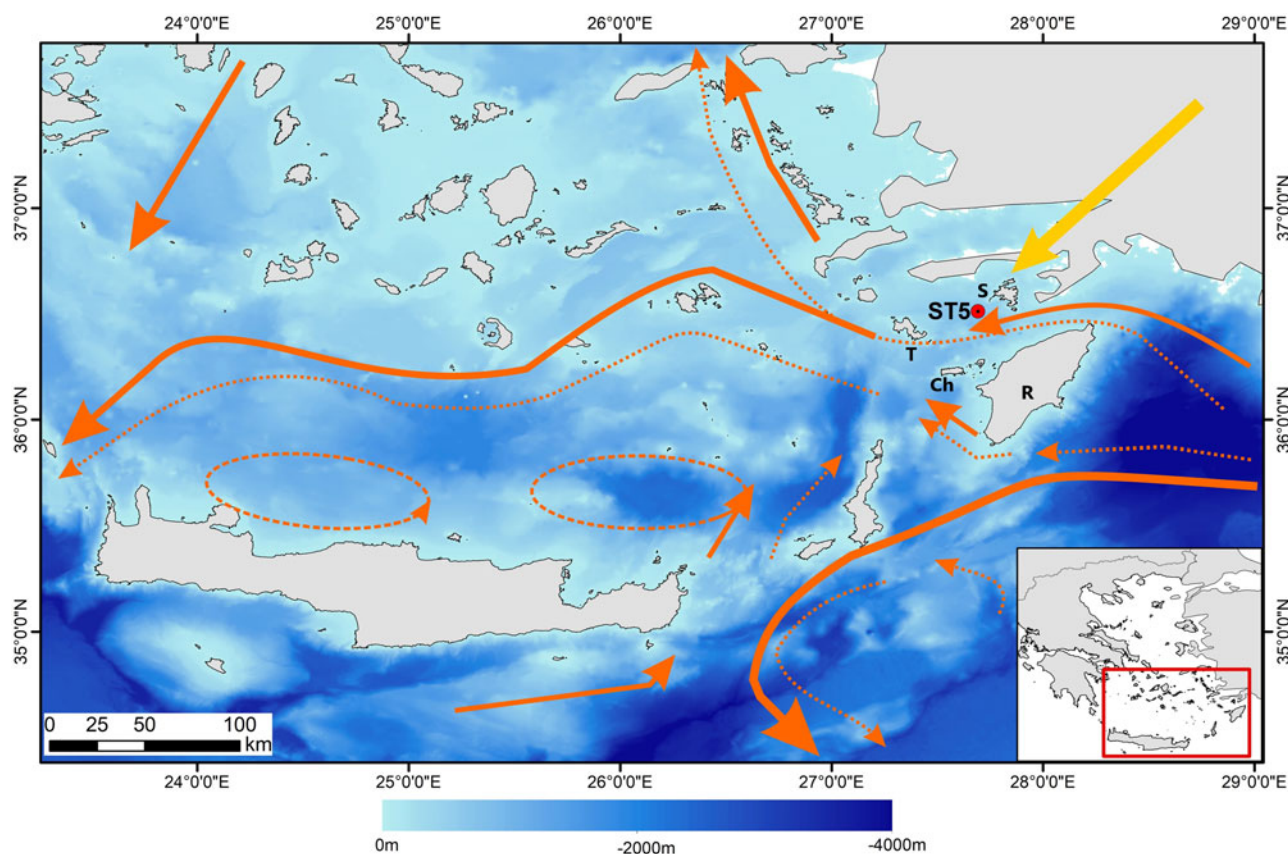


Fig. 11. Circulation of the surface waters (solid orange lines) and intermediate waters (dashed orange lines) (Estournel *et al.*, 2021) and major terrigenous sediment source path (yellow arrow) in the study area. Ch = Chalki Island; R = Rhodes Island; S = Symi Island; T = Tilos Island.

smectite content of ST5 sediments. Additionally, in this case, the smectite should have a low dehydroxylation temperature.

The presence of abundant chlorite in the ST5 sediments is indicative of limited weathering of the source rocks, which is typical of glacial erosion (Thiry, 2000). However, the abundance of chlorite is at odds with the low $\text{Al}_2\text{O}_3/\text{TiO}_2$ ratios, which indicate a humid climate during weathering, being favourable for the formation of kaolinite (Kiipli *et al.*, 2012). This apparent contradiction is compatible with close lithological control of the nearby source areas regarding the composition of the ST5 sediments. The presence of numerous ophiolite outcrops and metamorphic rocks in the nearby Lycian nappes of the west Anatolian landmass, as well as the widespread limestone and dolomite outcrops in the nearby Rhodes, Symi, Chalki and Tilos islands (Papanikolaou, 2021), may provide a solution to this apparent contradiction. The pattern of the $\text{Al}_2\text{O}_3/\text{TiO}_2$ ratios mimics those of the CIA values and illite contents, increasing towards the top of the sequence, whereas chlorite does not follow a clear trend with depth (Figs 3 & 8a). However, both serpentine and dolomite decrease gradually towards the top (Fig. 3), contributing to the decrease in MgO, Ni and Cr in the same direction (Fig. 8a,b). The observed mineralogical and geochemical trends suggest that the sediment composition is controlled by provenance rather than by climate. Indeed, clear climatic control over the distribution of clay minerals would have caused a decrease of the chlorite content to match the CIA values.

The observed decreases in the serpentine contents towards the top of the sequence, coupled with the decrease in the MgO, Ni, and Cr on the one hand and the increase in the illite, smectite

and Al_2O_3 contents, the CIA values and the $\text{Al}_2\text{O}_3/\text{TiO}_2$ ratios in the same direction on the other, are compatible with a gradual change in the source areas from an ophiolite-enriched source to a crustal-enriched source. Moreover, the gradual decrease in MgO is mimicked by the abundance of Mg-calcite in the sediments (Figs 3 & 8a). Although dissolved Mg^{2+} is released during weathering of ultramafics and/or dissolution of dolomites, seawater composition is buffered with respect to the major cations such as Mg^{2+} . The causes that triggered the gradual change in the sedimentation pattern are not known with certainty. A possible explanation might be a gradual transition to slightly drier climatic conditions, as indicated by the gradual increase in smectite and chlorite contents, the large particle sizes of chlorite and illite (mainly of coarse silt size) and the evolution of the $\text{Al}_2\text{O}_3/\text{TiO}_2$ ratios. In any case, the gradually increasing contribution of additional sources from the eastern Mediterranean Sea should be excluded for three reasons: (1) particle size remained essentially unchanged throughout the sedimentation column, being dominated by the coarse silt fraction; (2) the abundance of smectite – the main phase, which has been assumed to have a Nilotic origin (Ehrmann *et al.* 2007, 2013; Poulos 2009) – follows a similar distribution pattern to illite (Fig. 4 & inset in Fig. 8b), which has been transported from the west Anatolian mainland, suggesting a common source for the minerals; and (3) the abundance of key minerals such as chlorite, which is of local origin, remained relatively constant throughout the column.

Generally, in contrast to the C40 and TI13 cores from the south-west Aegean Sea and the Cretan Sea, respectively, the sapropel S1 sediments do not display significant differentiation

in mineralogical and geochemical composition. There are only a few exceptions, such as the C_{org} content, the increasing abundance of amphibole and the greater concentrations of certain trace elements such as V, Co and Ba, which led to a large Ba/Al ratio. Hence, the sedimentary influx did not fluctuate significantly during deposition of the sapropel, highlighting the control of the nearby landmasses over the sedimentary processes in the area during the entire time interval examined. These observations suggest that clay mineralogy based on traditional approaches and geochemical indices such as the CIA, the Al_2O_3/TiO_2 ratio or similar indices should be used with caution for climatic interpretations in relatively closed basins surrounded by large landmasses such as the Aegean Sea. Whilst such indices might be reliable for tracing aeolian provenance in terrains with limited riverine supply, such as the central and western Mediterranean Sea (Bout-Roumazeilles *et al.*, 2007, 2013), they are of limited importance in the Aegean Sea, which is surrounded by large landmasses and the sedimentary record of which is dominated by considerable river supply, especially in the eastern and northern Aegean coasts.

Conclusions

The clay mineralogy and the geochemical record of sediments recovered from core ST5 in the south-east Aegean Sea showed evidence of substantial terrigenous input. By contrast, the accumulation of calcium carbonate in the marine sediments, which is mainly controlled by the productivity in the euphotic zone, is limited compared to the south-west Aegean Sea and the Cretan Sea, emphasizing the influence of the terrigenous supply of sediments from the nearby landmasses. The sediments are characterized by chlorite as the principal clay mineral and the presence of minor serpentine and amphibole as key tracer minerals, aiding in determining the provenance of the sediments. The geochemical fingerprinting of the sediments is dominated by abundant MgO, Ni, Cr and Co, which, in association with the mineralogical signature, indicate supply from an ultrabasic source, probably the Marmaris ophiolite in the Lycian nappes.

Similar to the sediments from the Cretan Sea (Leontopoulou *et al.*, 2019), the input of material from the south-east Mediterranean Sea seems to be of minor importance in the studied column, rendering previous suggestions for the origin of clay minerals questionable at least. Moreover, quantitative analysis of the non-clay fraction using reliable methods such as Rietveld refinement provides important information about the provenance of sediments, which are not traceable using traditional methods due to analytical constraints. Hence, in sedimentary environments characterized by controlled exchange with larger basins and sediment supply from the surrounding landmasses, quantitative bulk mineralogy coupled with analysis of the dehydroxylation behaviour of certain clay minerals, such as smectite, can be useful tools for tracing sediment provenance and may enable a more realistic assessment of the importance of water circulation patterns for sedimentation processes.

Supplementary material. To view supplementary material for this article, please visit <https://doi.org/10.1180/clm.2022.2>.

Acknowledgements. A. Stratakis assisted with the XRD analysis. E. Koutsopoulou assisted with the SEM work and E. Chamilaki with the CHNS measurements.

References

- Adriaens R., Zeelmaekers E., Fettweis M., Vanlierde E., Vanlede J., Stassen P. *et al.* (2018) Quantitative clay mineralogy as provenance indicator for recent muds in the southern North Sea. *Marine Geology*, **398**, 48–58.
- Aksu A.E., Yaşar D. & Mudie P.J. (1995a) Origin of late glacial–Holocene hemipelagic sediments in the Aegean Sea: clay mineralogy and carbonate cementation. *Marine Geology*, **123**, 33–59.
- Aksu A.E., Yaşar D., Mudie P.J. & Gillespie H. (1995b) Late glacial–Holocene paleoclimatic and paleoceanographic evolution of the Aegean Sea: micropaleontological and stable isotopic evidence. *Marine Micropaleontology*, **25**, 1–28.
- Bayhan E., Ergin M., Temel A. & Keskin Ş. (2001) Sedimentology and mineralogy of surficial bottom deposits from the Aegean–Çanakkale–Marmara transition (eastern Mediterranean): effects of marine and terrestrial factors. *Marine Geology*, **175**, 297–315.
- Biscaye P.E. (1965) Mineralogy and sedimentation of recent deep-sea clay in the Atlantic Ocean and adjacent seas and oceans. *Geological Society of America Bulletin*, **76**, 803–832.
- Bish D.L. & Plötze M. (2011) X-ray powder diffraction with emphasis on qualitative and quantitative analysis in industrial mineralogy. Pp. 35–76 in: *Advances in the Characterization of Industrial Minerals*. EMU Notes in Mineralogy 9 (G.E. Christidis, editor). European Mineralogical Union and the Mineralogical Society of Great Britain and Ireland, London, UK.
- Borchard G. (1989) Smectites. Pp. 675–727 in: *Minerals in Soil Environments*, 2nd ed. (J.B. Dixon & S.B. Weed, editors). Soil Science Society of America, Madison, WI, USA.
- Bout-Roumazeilles V., Combourieu Nebout N., Desprat S., Siani G., Turon J.-L. & Essallami L. (2013) Tracking atmospheric and riverine terrigenous supplies variability during the last glacial and the Holocene in central Mediterranean. *Climate of the Past*, **9**, 1065–1087.
- Bout-Roumazeilles V., Combourieu Nebout N., Peyron O., Cortijo E., Landais A. & Masson-Delmotte V. (2007) Connection between south Mediterranean climate and North African atmospheric circulation during the last 50,000 yr bp North Atlantic cold events. *Quaternary Science Reviews*, **26**, 3197–3215.
- Caquineau S., Gaudichet A., Gomes L., Magonthier M. & Chatenet B. (1998) Saharan dust: clay ratio as a relevant tracer to assess the origin of soil-derived aerosols. *Geophysical Research Letters*, **25**, 983.
- Chamley H. (1989) *Clay Sedimentology*. Springer Verlag, Berlin, Germany, 623 pp.
- Christidis G.E. (2006) Genesis and compositional heterogeneity of smectites. Part III. Alteration of basic pyroclastic rocks. A case study from the Troodos Ophiolite Complex, Cyprus. *American Mineralogist*, **91**, 685–701.
- Christidis G.E. & Mitsis I. (2006) A new Ni-rich stevensite from the ophiolite complex of Othrys, central Greece. *Clays and Clay Minerals*, **54**, 653–666.
- Christidis G.E. & Skarpelis N. (2010) Clay mineralogy of the sedimentary iron–nickel ore of Agios Ioannis, NE Boeotia: new data and implications for diagenetic modifications. *Bulletin of the Geological Society of Greece*, **43**, 2553–2561.
- Christidis G.E., Perdikatsis V. & Apostolaki C. (2010) Mineralogy of the Saharan aeolian dust in Crete: examples from the period 2004–2009. *Bulletin of the Geological Society of Greece*, **43**, 2570–2576.
- Coudé-Gaussen G., Hillaire-Marcel C. & Rognon P. (1982) Origine et évolution pédologique des fractions carbonatées dans les loess des Matmata (Sud-Tunisien) d'après leurs teneurs en ^{13}C et ^{18}O . *Comptes Rendus de l'Académie des Sciences de Paris*, **295**, 939–942.
- Decarreau A., Colin F., Herbillon A., Manceau A., Nahon D., Paquet H. *et al.* (1987) Domain segregation in Ni–Fe–Mg smectites. *Clays and Clay Minerals*, **35**, 1–10.
- Deer W.A., Howie R.A. & Zussman J. (2013) *Rock Forming Minerals*, 3rd ed. The Mineralogical Society, London, UK, 498 pp.
- Dera G., Pellenard P., Neige P., Deconinck J.F., Pucéat E. & Dommergues J.L. (2009) Distribution of clay minerals in Early Jurassic Peritethyan seas: palaeoclimatic significance inferred from multiproxy comparisons. *Palaeogeography, Palaeoclimatology, Palaeoecology*, **271**, 39–51.
- Drits V.A., Eberl D.D. & Śródoń J. (1998) XRD measurement of mean thickness, thickness distribution and strain for illite and illite–smectite crystallites by the Bertaut–Warren–Averbach technique. *Clays and Clay Minerals*, **46**, 38–50.

- Ehrmann W., Schmiedl G., Hamann Y., Kuhnt T., Hemleben C. & Siebel W. (2007) Clay minerals in late glacial and Holocene sediments of the northern and southern Aegean Sea. *Palaeogeography, Palaeoclimatology, Palaeoecology*, **249**, 36–57.
- Ehrmann W., Seidel M. & Schmiedl G. (2013) Dynamics of late Quaternary North African humid periods documented in the clay mineral record of central Aegean Sea sediments. *Global Planetary Change*, **107**, 186–195.
- Ergin M., Bayhan E. & Temel A. (2012) Clay mineral distribution in last glacial–Holocene sediment cores from the eastern Marmara Sea (Çınarcık Basin–Izmit Gulf transition), NW-Turkey: multisources and transport paths in a two-way flow system. *Quaternary International*, **261**, 53–74.
- Ergin M., Kadir S., Keskin Ş., Turhan-Akyüz N. & Yaşar D. (2007) Late Quaternary climate and sea-level changes recorded in sediment composition off the Büyük Menderes River delta (eastern Aegean Sea, Turkey). *Quaternary International*, **167–168**, 162–176.
- Estournel C., Marsaleix P. & Ulses C. (2021) A new assessment of the circulation of Atlantic and Intermediate Waters in the Eastern Mediterranean. *Progress in Oceanography*, **198**, 102673.
- Facorellis Y., Maniatis Y. & Kromer B. (1998) Apparent ^{14}C ages of marine mollusk shells from a Greek island: calculation of the marine reservoir effect in the Aegean Sea. *Radiocarbon*, **40**, 963–973.
- Filippidi A., Triantaphyllou M.V. & De Lange G.J. (2016) Eastern-Mediterranean ventilation variability during sapropel S1 formation, evaluated at two sites influenced by deep-water formation from Adriatic and Aegean seas. *Quaternary Science Reviews*, **144**, 95–106.
- Folk R.L. (1974) *Petrology of Sedimentary Rocks*. Hemphill Publishing Co., Austin, TX, USA, 170 pp.
- Fontaine F., Christidis G.E., Yans J., Hollanders S., Hoffman A. & Fagel N. (2020) Characterization and origin of two Fe-rich bentonites from Westerwald (Germany). *Applied Clay Science*, **187**, 105444.
- Garzanti E., Padoan M., Setti M., López-Galindo A. & Villa I.M. (2014) Provenance versus weathering control on the composition of tropical river mud (southern Africa). *Chemical Geology*, **366**, 61–74.
- Gaudin A., Grauby O., Noack N., Decarreau A. & Petit S. (2004) Accurate crystal chemistry of ferric smectites from the lateritic nickel ore of Murrin Murrin (Western Australia). I. XRD and multi-scale chemical approaches. *Clay Minerals*, **39**, 301–315.
- Georgakopoulou M., Hein A., Müller N.S. & Kiriati E. (2017) Development and calibration of a WDXRF routine applied to provenance studies on archaeological ceramics. *X-Ray Spectrometry*, **46**, 186–199.
- Geraga M., Tsaila-Monopolis S., Ioakim C., Papatheodorou G. & Ferentinos G. (2000) Evaluation of palaeoenvironmental changes during the last 18,000 years in the Myrtoon Basin, SW Aegean Sea. *Palaeogeography, Palaeoclimatology, Palaeoecology*, **156**, 1–17.
- Gogou A., Bouloubassi L., Lykousis V., Arnaboldi M., Gaitani P. & Meyers P.A. (2007) Organic geochemical evidence of late glacial–Holocene climate instability in the north Aegean Sea. *Palaeogeography, Palaeoclimatology, Palaeoecology*, **256**, 1–20.
- Güngör T., Akal C., Özer S., Hasözbeke A., Sarı B. & Mertz-Kraus R. (2018) Kinematics and U–Pb zircon ages of the sole metamorphics of the Marmaris ophiolite, Lycian nappes, southwest Turkey. *International Geology Review*, **61**, 1124–1142.
- Güzel N. & Wilson M.J. (1981) Clay-mineral studies of a soil chronosequence in southern Turkey. *Geoderma*, **20**, 113–129.
- Hughen K.A., Baillie M.G.L., Bard E., Warren Beck J., Bertrand C.J.H., Blackwell P.G. et al. (2004) Marine04 marine radiocarbon age calibration, 0–26 cal bp. *Carbon*, **46**, 1059–1086.
- Kadir S., Eren M., Külah T., Önalğıl N., Cesur M. & Gürel A. (2014) Genesis of Late Miocene–Pliocene lacustrine palygorskite and calcretes from Kırşehir, central Anatolia, Turkey. *Clay Minerals*, **49**, 473–494.
- Karageorgis A.P., Anagnostou C.L. & Kaberi H. (2005) Geochemistry and mineralogy of the NW Aegean Sea surface sediments: implications for river runoff and anthropogenic impact. *Applied Geochemistry*, **20**, 69–88.
- Karageorgis A.P., Kanellopoulos T.D., Mavromatis V., Anagnostou C.L., Koutsopoulou E., Schmidt M. et al. (2012) Authigenic carbonate mineral formation in the Pagassitikos palaeolake during the latest Pleistocene, central Greece. *Geo-Marine Letters*, **33**, 13–29.
- Kemp S.J., Ellis M.A., Mountney I. & Kender S. (2016) Palaeoclimatic implications of high-resolution clay mineral assemblages preceding and across the onset of the Palaeocene–Eocene thermal maximum, North Sea Basin. *Clay Minerals*, **51**, 793–813.
- Kiipli E., Kiipli T., Kallaste T. & Siir S. (2012) $\text{Al}_2\text{O}_3/\text{TiO}_2$ ratio of the clay fraction of Late Ordovician–Silurian carbonate rocks as an indicator of paleoclimate of the Fennoscandian Shield. *Palaeogeography, Palaeoclimatology, Palaeoecology*, **365–366**, 312–320.
- Kronberg B.I., Nesbitt H.W. & Lam W.W. (1986) Upper Pleistocene deep-sea fan muds reflect chemical weathering of their mountainous source lands. *Chemical Geology*, **54**, 283–294.
- Leontopoulou G., Christidis G.E., Geraga M., Papatheodorou G. & Koutsopoulou E. (2019) A novel mineralogical approach for provenance analysis of late Quaternary marine sediments: the case of Myrtoon Basin and Cretan Sea, Aegean, Greece. *Sedimentary Geology*, **384**, 70–84.
- Lister C.J., Hiscott R.N., Aksu A.E. & Mudie P.J. (2015) Compositional trends through the Holocene mud succession of the southwestern Black Sea shelf: implications for sedimentary provenance and water-level history. *Sedimentary Geology*, **316**, 13–25.
- Lykousis V., Chronis G., Tselepidis A., Price N.B., Theocharis A., Siokou-Frangou I. et al. (2002) Major outputs of the recent multidisciplinary biogeochemical researches undertaken in the Aegean Sea. *Journal of Marine Systems*, **33–34**, 313–334.
- Mano E.S., Caner L., Petit S., Chaves A.P. & Mexias A.S. (2014) Mineralogical characterisation of Ni-bearing smectites from Niquelândia, Brazil. *Clays and Clay Minerals*, **62**, 324–335.
- Martinez-Ruiz F., Kastner M., Paytan A., Ortega-Huertas M. & Bernasconi S.M. (2000) Geochemical evidence for enhanced productivity during S1 sapropel deposition in the eastern Mediterranean. *Paleoceanography*, **15**, 200–209.
- McLennan S.M., Hemming S., McDaniel D.K. & Hanson G.L. (1993) Geochemical approaches to sedimentation, provenance, and tectonics. *Special Papers – Geological Society of America*, **285**, 21–40.
- Mercione D., Thomson J., Abu-Zied I.R.H., Croudace W. & Rohling E.J. (2001) High-resolution geochemical and micropalaeontological profiling of the most recent eastern Mediterranean sapropel. *Marine Geology*, **177**, 25–44.
- Meunier A., Caner L., Hubert F., El Albani A. & Pret D. (2013) The weathering intensity scale (WIS): an alternative approach of the Chemical Index of Alteration (CIA). *American Journal of Science*, **313**, 113–143.
- Molinaroli E. (1996) Mineralogical characterization of Saharan dust with a view to its final destination in Mediterranean sediments. Pp. 153–162 in: *The Impact of Desert Dust across the Mediterranean* (S. Guerzoni & R. Chester, editors). Kluwer Academic, Dordrecht, The Netherlands.
- Munoz M., Ulrich M., Cathelineau M., & Mathon O. (2019) Weathering processes and crystal chemistry of Ni-bearing minerals in saprock horizons of New Caledonia ophiolite. *Journal of Geochemical Exploration*, **198**, 82–99.
- Nesbitt H.W. & Young G.M. (1982) Early Proterozoic climates and plate motions inferred from major elements chemistry of lutites. *Nature*, **299**, 715–717.
- Özkan A. & Ross G.J. (1979) Ferruginous beidellites in Turkish soils. *Soil Science Society of America Journal*, **43**, 1242–1248.
- Papanikolaou D.I. (2021). *The Geology of Greece*. Springer International Publishing, Berlin, Germany, 345 pp.
- Parlak O. (2016) The tauride ophiolites of Anatolia (Turkey): a review. *Journal of Earth Science*, **27**, 901–934.
- Pinardi N. & Masetti E. (2000) Variability of the large scale general circulation of the Mediterranean Sea from observations and modelling: a review. *Palaeogeography, Palaeoclimatology, Palaeoecology*, **158**, 153–173.
- Post J.E. & Bish D.L. (1989) Rietveld refinement of crystal structures using powder X-ray diffraction data. Pp. 277–308 in: *Modern Powder Diffraction*. Reviews in Mineralogy 20 (D.L. Bish & J.E. Post, editors). De Gruyter, Berlin, Germany.
- Poulos S.E. (2009) Origin and distribution of the terrigenous component of the unconsolidated surface sediment of the Aegean floor: a synthesis. *Continental Shelf Research*, **29**, 2045–2060.
- Reimer P.J. & McCormac F.G. (2002) Marine radiocarbon reservoir corrections for the Mediterranean and Aegean seas. *Radiocarbon*, **44**, 159–166.
- Rousakis G., Karageorgis A.P., Conispoliatis N. & Lykousis V. (2004) Last glacial–Holocene sediment sequences in N. Aegean basins: structure, accumulation rates and clay mineral distribution. *Geo-Marine Letters*, **24**, 97–111.

- Sabatier P., Dezileau L., Briquieu L., Colin C. & Siani G. (2010) Clay minerals and geochemistry record from northwest Mediterranean coastal lagoon sequence: implications for paleostorm reconstruction. *Sedimentary Geology*, **228**, 205–217.
- Shaw H.F. & Bush P.R. (1978) The mineralogy and geochemistry of the Recent surface sediments of the Cilicia Basin, northeast Mediterranean. *Marine Geology*, **27**, 115–136.
- Snellings R., Machiels L., Mertens G., & Elsen J. (2010) Rietveld refinement strategy for quantitative phase analysis of partially amorphous zeolitized tuffaceous rocks. *Geologica Belgica*, **13**, 183–196.
- Stuiver M. & Reimer P.J. (1993) Extended C-14 data-base and revised Calib 3.0 C-14 age calibration program. *Radiocarbon*, **35**, 215–230.
- Stuiver M., Reimer P.J., Bard E., Beck J.W., Burr G.S., Hughen K.A. *et al.* (1998) INTCAL98 radiocarbon age calibration, 24,000–0 cal bp. *Radiocarbon*, **40**, 1041–1083.
- Thiry M. (2000) Palaeoclimatic interpretation of clay minerals in marine deposits: an outlook from the continental origin. *Earth-Science Reviews*, **49**, 201–221.
- Thomson J., Nixon S., Summerhayes C.P., Schönfeld J., Zahn R. & Grootes P.M. (1999) Sedimentology and geochemistry of the Iberian margin. Pangaea. Available at: <https://doi.org/10.1594/PANGAEA.735613>
- Triantaphyllou M.V., Ziveri P., Gogou A., Marino G., Lykousis V., Bouloubassi I. & Nunez N. (2009) Late glacial–Holocene climate variability at the south-eastern margin of the Aegean Sea. *Marine Geology*, **266**, 182–197.
- Tripanas E.K., Panagiotopoulos I.P., Lykousis V., Morfis I., Karageorgis A.P., Anastasakis G. & Kontogonis G. (2016) Late Quaternary bottom-current activity in the south Aegean Sea reflecting climate-driven dense-water production. *Marine Geology*, **375**, 99–119.
- Vanderaverroet P., Averbuch O., Deconinck J.F. & Chamley H. (1999) A record of glacial/interglacial alternations in Pleistocene sediments off New Jersey expressed by clay mineral, grain-size and magnetic susceptibility data. *Marine Geology*, **159**, 79–92.
- Van Santvoort P.J.M., de Lange G.J., Thomson J., Cussen H., Wilson T.R.S., Krom M.D. & Ströhle K. (1996) Active post-depositional oxidation of the most recent sapropel (S1) in sediments of the eastern Mediterranean Sea. *Geochimica et Cosmochimica Acta*, **60**, 4007–4017.
- Venkatarathnam K. & Ryan W.B.F. (1971) Dispersal patterns of clay minerals in the sediments of the eastern Mediterranean Sea. *Marine Geology*, **11**, 261–282.
- Villanova-De-Benavent C., Domènech C., Tauler E., Galí S., Tassara S. & Proenza J.A. (2017) Fe–Ni-bearing serpentines from the saprolite horizon of Caribbean Ni-laterite deposits: new insights from thermodynamic calculations. *Mineralium Deposita*, **52**, 979–992.
- Weir A.H., Ormerod E.C. & El Mansey I.M. (1975) Clay mineralogy of sediments of the western Nile Delta. *Clay Minerals*, **10**, 369–386.
- Wentworth C.K. (1922) A scale of grade and class terms for clastic sediments. *Journal of Geology*, **30**, 377–392.
- Wilson M.J. (1999) The origin and formation of clay minerals in soils: past, present and future perspectives. *Clay Minerals*, **34**, 7–25.
- Yilmaz A. & Yilmaz H. (2013) Ophiolites and ophiolitic mélanges of Turkey: a review. *Geological Bulletin of Turkey*, **56**, 65–114.
- Zalasiewicz J., Williams M., Haywood A. & Ellis M. (2011) The Anthropocene: a new epoch of geological time? *Philosophical Transactions of the Royal Society A: Mathematical, Physical and Engineering Sciences*, **369**, 835–841.
- Zeelmaekers E., Honty M., Derkowski A., Srodon J., De Craen M., Vandenberghe N.R. *et al.* (2015) Qualitative and quantitative mineralogical composition of the Rupelian Boom Clay in Belgium. *Clay Minerals*, **50**, 249–272.